International Journal of Earth Sciences
https://doi.org/10.1007/s00531-022-02247-5

ORIGINAL PAPER

Late Carboniferous Schlingen in the Gotthard nappe (Central Alps) and their relation to the Variscan evolution

M. Bühler[1] · R. Zurbriggen[1] · A. Berger[1] · M. Herwegh[1] · D. Rubatto[1]

Received: 14 June 2022 / Accepted: 8 September 2022

Abstract
Pre-Mesozoic basements of the Alpine belt commonly contain kilometre-scale folds with steeply inclined axial planes and fold axes, which are named "Schlingen" folds. The structural evolution of Schlingen folds and their geodynamic significance for the Variscan evolution are unclear. To close this gap, this study investigates a well-preserved Schlingen structure in the Gotthard nappe (Central Swiss Alps). This Schlingen fold evolved by a combination of shearing and folding under amphibolite-facies conditions. Detailed digital field mapping, coupled with petrographical and structural investigations, reveal local synkinematic migmatisation in the fold hinges parallel to axial planes. Zircon crystals from leucosomes in the fold hinges have magmatic cores that yield an age of 449 ± 3 Ma, and rims with a range of dates from ~ 270 to 330 Ma (main cluster at 315 ± 4 Ma). We ascribe this late Carboniferous age to peak metamorphic conditions of the late Variscan Schlingen phase. Moreover, we describe for the first time post-Schlingen, but pre-Alpine transpressional deformation. The investigated Schlingen fold is discussed with respect to comparable structures of the wider Alpine realm, located in the most southern part of the Variscan belt. We propose that Schlingen formation concurred with the crustal-scale transpressional tectonics. This scenario separates, at least in a structural sense, the Southern Variscides from more northern parts (also Gondwana derived), where Schlingen folds are absent.

Keywords Crustal-scale folds with steep axes · Schlingen · Variscan tectonics · Alps · U–Pb dating · Orocline

Introduction

Many of the pre-Mesozoic polycyclic metamorphic basement units of the Alps contain steeply oriented kilometre-scale folds (Zurbriggen 2015). These characteristic, yet intriguing, large-scale structures have evoked various and controversial hypotheses about their genesis and recurrent abundance within the Alpine belt (e.g. Sander 1914; Andreatta 1948; van Gool et al. 1987; Zurbriggen et al. 1998). There exists still no generally accepted model to explain these Variscan tectono-metamorphic features and thus their potential significance for deformation at the low to mid crustal transition is poorly understood. Previous studies refer to these map-scale structures as steep folds in the Pfossental (Austria) and Silvretta nappe (Sander 1914; Spitz and Dyhrenfurth 1914), vortex structures in the Schneeberg complex (Andreatta 1948; Förster 1967), large-scale subvertical folds in the Aiguilles Rouges Massif (von Raumer and Bussy 2004), asymmetric open folds in the Tonale nappe (Martin et al. 1998; Moro et al. 1999) and Schlingen folds. The latter are described in the southern Oetztaler Alps (Schmidt 1964, 1965; Van Gool et al. 1987; Zanchetta 2010), between Tonale and Ultental, in the southern Defereggen Alps (Schmidegg 1936; Schmidt 1965; Schulz 1988) and the Strona-Ceneri zone (Boriani et al. 1990; Zurbriggen et al. 1998). Schlingen are also described in the Aar Massif (Abrecht 1994) and the Gotthard nappe (Huber 1943). For this study we choose the German term *Schlingen* (Schlingen folds or Schlingen structure) to encompass all structures

✉ M. Bühler
buehlermario@gmail.com

R. Zurbriggen
roger-zurbriggen@bluewin.ch

A. Berger
alfons.berger@geo.unibe.ch

M. Herwegh
marco.herwegh@geo.unibe.ch

D. Rubatto
daniela.rubatto@geo.unibe.ch

[1] Institute of Geological Science, University of Bern, Baltzerstrasse 1+3, CH-3012 Bern, Switzerland

Published online: 15 October 2022

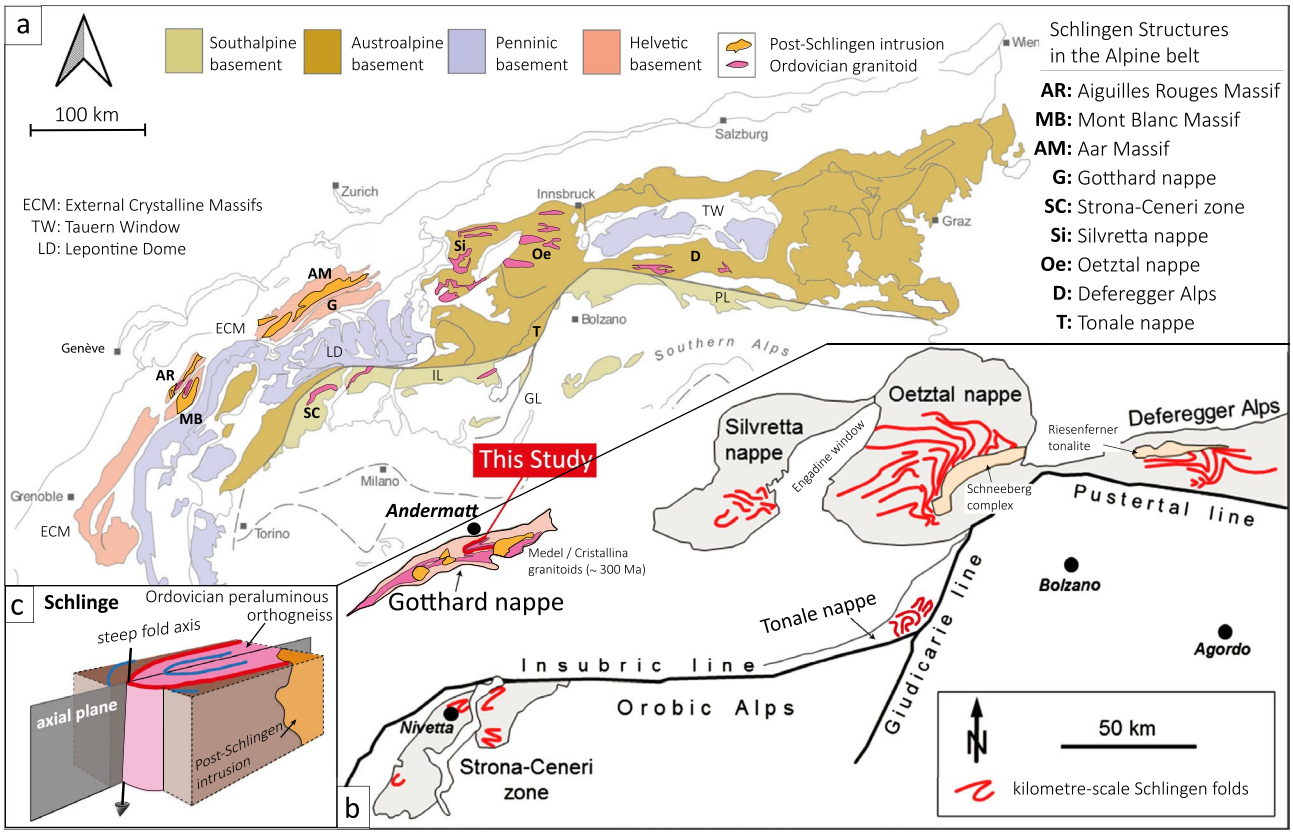

Fig. 1 Schlingen structures in the Alps. **a** Compilation map of pre-Permian Schlingen containing polycyclic metamorphic basement units in the Alpine belt. Associated and extensively outcropping Ordovician granitoids and post-Schlingen intrusions (late Carboniferous to early Permian) constrain a time frame for the Schlingen phase. **b** Compilation map of the described Schlingen structures of the Gotthard nappe and Austroalpine and Southalpine basement units. **c** Simplified block model of a Schlingen vertical fold with a steep fold axis and steep axial plane. **a** Modified after von Raumer et al. (2013). Ordovician granitoids also occur in the Penninic units (Table S1 in Ballèvre et al. 2018). Here, they are only shown for the Eastern and Southalpine units. **b** Modified after Zurbriggen (2015)

irrespective of their magnitude from map scale to micro-scale, caused by the Schlingen event or Schlingen phase (Bächlin 1937). As its descriptive manifold terminology suggests, Schlingen are large-scale folds with a distinctively steep axial plane and corresponding moderately to steeply plunging fold axis (30°–90° e.g. Schaltegger 1984; Spiess et al. 2010). Schlingen folds always deform steeply inclined pre-Variscan foliations and occur throughout the Alpine belt (see above, Fig. 1a). Most authors mapped tight, isoclinal folds with acute interlimb angles (Fig. 1b), but some rather open folds are also reported (Zurbriggen et al. 1998; Moro et al. 1999), as well as moderately inclined Schlingen folds that deform flatter pre-existing structures (Van Gool et al. 1987). Paleozoic structures are best exposed in polycyclic metamorphic basement units devoid of penetrative Alpine overprint, where peak metamorphic conditions are related to the Schlingen or previous phases. Kilometre-scale Schlingen folds form at amphibolite-facies conditions (Schaltegger 1984; Schulz 1988; Mercolli et al. 1994; Sölva et al. 2005). Schlingen folds deform the Ordovician orthogneisses and are truncated by early-Permian to late Carboniferous intrusives (Schmidegg 1936; Mercolli et al. 1994, also see Fig. 1c). In the Strona-Ceneri zone, they are discordantly overlain by unmetamorphosed Permo-Carboniferous sediments (Zingg et al. 1990). These crosscutting relationships limit a maximum time frame for Schlingen formation between 450 and 310 Ma. Schlingen structures are widely accepted to be of pre-Permian age (e.g. Wenk 1934; Huber 1943; Zurbriggen et al. 1998).

Furthermore, Schlingen may show interferences with superimposed later-stage minor deformation events (Schmidegg 1936; Zurbriggen et al. 1998; Sölva et al. 2001; Zanchetta 2010). Palinspastic reconstructions of pre-Alpine basements reveal that several tectonic domains were spatially closely related prior to onset of Variscan shear tectonics (e.g. Ballèvre et al. 2018; Jouffray et al. 2020). Since Schlingen folds are equally observed in the external crystalline massif, the Austroalpine and Southalpine basements, their abundance suggests a common tectonomorphic deformation style that had a profound and regional impact

on pre-Alpine intra-Pangea units. In the Austroalpine basements, the formation of Schlingen folds has been related to dextral transpressional tectonics during the Namurian–Westphalian convergence (Schulz et al. 2008; Spiess et al. 2010). Von Raumer et al. (2013) attributed Schlingen folds to large-scale strike-slip tectonics.

The central part of the Gotthard nappe in southern Switzerland represents an ideal area to study the complex Paleozoic deformation history, since pre-Mesozoic structures are well preserved and Alpine deformational overprint is limited (Mercolli et al. 1994; Berger et al. 2017). Because of its strategic geographic position along a main north–south European route, multiple tunnels have been constructed in the Gotthard region. The numerous construction reports describing lithologies, tectonics and geotechnical properties of drilled rock units have contributed to compilation of geological maps (e.g. Mercolli et al. 1994; Labhart 2005; Labhart and Renner 2012; Berger et al. 2017; Rast et al. 2022) and kinematic models (Pfiffner 2006; Herwegh et al. 2017, 2020; Ricchi et al. 2019).

In this study, we present structural, petrographic and geochronological data of an indicative, yet most exemplary Schlingen structure of the Central Alps in the Gotthard nappe. Since Schlingen fabrics are observed at various scales, we use a multi-perspective approach incorporating digital field mapping, thin section analysis and isotope dating. We then discuss the implication and potential significance of the Schlingen structures for mid to lower crustal deformation.

Geological setting

The investigated study area is located in the basement of the Gotthard nappe (Central Alps, Switzerland). The Gotthard nappe is characterised by pre-Alpine basement surrounded by Mesozoic metasediments. In the Alpine structure, the basement represents the lithological core of the nappe. These basement units have been historically subdivided into pre-Variscan basement, Variscan structures and post-Variscan plutonic units (see below). In the following, the pre-Variscan and Variscan evolution are summarised, whereas the Mesozoic and Alpine evolution is only mentioned shortly (not a topic of this contribution).

Prior to the onset of the Variscan orogeny, the early Paleozoic basement of the future Alps was located within the peri-Gondwana terrains (e.g. Guillot and Ménot 2009; Ballèvre et al. 2018). The Gotthard nappe and the adjacent Aar Massif consist of polycyclic metamorphic basement units that record the pre-Mesozoic history of the Central Alps (e.g. Abrecht 1994; Mecolli et al. 1994; Schaltegger 1994; Ballèvre et al. 2014). The basement of the nappe is mainly composed of paragneisses with migmatitic derivatives and intercalated amphibolites, calcsilicates, ultramafic rocks and orthogneisses (Mercolli et al. 1994; Berger et al. 2017). The formation of eclogites at ~ 470 Ma was followed by an amphibolite- to granulite-facies high-temperature metamorphism that led to partial melting (e.g. Biino and Mercolli 1991; Abrecht 1994); the corresponding migmatites are exposed in the Paradis Gneiss Complex (Berger et al. 2017). The Ordovician–Silurian cycle is sealed by the emplacement of peraluminous and calc-alkaline orthogneisses (Ordovician metagranitoids in Fig. 1a). In the Gotthard nappe, the intrusion of the protolith of the Streifengneis is dated at 439 ± 5 Ma (Sergeev and Steiger 1993). The tectonometamorphic setting for the formation of the early Paleozoic, pre-Variscan gneisses is debated. Abrecht et al. (1991) and Schaltegger (1994) proposed a Cambrian–Ordovician cordillera-type orogenic cycle. According to Biino and Mercolli (1991) and Abrecht (1994), eclogites indicate a subduction-related metamorphism followed by collision. Schulz and Raumer (2011) and von Raumer et al. (2013) interpreted the Ordovician anatexis and magmatism in the context of crustal thinning and rifting of the Rheic basin. Zurbriggen (2015) infers an active margin scenario of cratonising subduction-accretion complexes at the periphery of Gondwana, for which the new term Cenerian orogeny is proposed (Zurbriggen 2017).

In the context of the late Ordovician to middle Devonian rifting of the Paleotethys, the Gotthard nappe was exhumed as indicated by the deposition of clastic sediments of the Val Rondadura Group (Huber 1943; Niggli 1944; Von Raumer et al. 2013). Bonin et al. (1993) interpret the Val Rondadura Group as molasse-type deposits in an intracontinental basins created by short-lived transpressional or tensional regimes during a post-collisional stage of exhumation, mainly during Devonian and Carboniferous times.

The onset of the Variscan orogeny was marked by the lower- to middle Devonian (400–380 Ma; Eo-Variscan) collision of northwards drifting Gondwanan Eastern Shelf with Laurussia (von Raumer and Neubauer 1993; Stampfli and Borel 2002; Guillot et al. 2009). The uppermost Devonian to Visean Meso-Variscan event (360–330 Ma) was characterised by subduction—accretion and nappe stacking (Guillot and Ménot 2009). Subsequently, during a Pennsylvanian Neo-Variscan event (330–310 Ma) orogen-wide transpression dominated (Putiš et al. 2009; Stampfli and Hochard 2009; Von Raumer et al. 2013; Haas et al. 2020). This Variscan evolution is well described for basements outside the Alps like the Black Forest (e.g. Schaltegger 2000), the Central Massif (Faure et al. 2017) and the Iberian Peninsula (Martínez Catalan et al. 2007). Variscan relics are also prominent in the External Crystalline Massif of the Alpine belt (e.g. Guillot and Ménot 2009; Bussien et al. 2011; Ballèvre et al. 2018; Fréville et al. 2018). In this region, syn- to post-orogenic intrusions of predominant

granitic composition preserve different evolution stages of the Variscan orogeny between 330 and 290 Ma (late Carboniferous intrusion, e.g. Schaltegger and Corfu 1995; Sergeev et al. 1995; von Raumer and Bussy 2004; Manzotti et al. 2012). Von Raumer and Bussy (2004) attributed the latest intrusions in the Mont Blanc Massif to crustal thinning and mantle uplift that resulted in pull-apart structure during Variscan strike-slip tectonics. Stephanian–Permian extension and crustal-scale strike-slip faulting are recorded in the western External Crystalline Massif (Malavieille et al. 1990; Gardien et al. 1997; Guillot and Ménot 2009), of which the East Variscan Shear Zone (EVSZ after Ballèvre et al. 2018; Jouffray et al. 2020) is a prominent feature.

During Alpine orogeny, the pre-Triassic basement units were thrusted and exhumed as the Gotthard nappe (Berger et al. 2011, 2017; Herwegh et al. 2020). The associated greenschist assemblage (Frey et al. 1999) and the very restricted and localised brittle–ductile Alpine deformation structures (Arnold 1972; Pettke and Klaper 1992; Etter et al. 1999; Lützenkirchen 2002; Zangerl et al. 2006) can be clearly distinguished from the pre-Alpine high-grade metamorphic events.

Methods

Mapping

The central part of the Gotthard nappe in southern Switzerland is an ideal place to study the complex Paleozoic deformation history, since pre-Mesozoic structures are well preserved (Mercolli et al. 1994; Berger et al. 2017) and only marginally overprinted by Alpine features. The study area is located at the southern end of the Unteralp Valley southeast of Andermatt (Fig. 2).

Even though Schlingen are defined as kilometre-scale structures, the identification of many of their indicative lithostructural features (e.g. axial plane parallel dyking, migmatisation and foliation spacing) requires a resolution that is between the outcrop scale and the scale of a regional geological map. Therefore, our 1: 5000 geological map covering an area of 10 km^2 sheds new light on the spatio-structural relationships. It visualises in detail the complex geology of the hinge zone of the kilometre-scale Tros Schlinge (Fig. 2a). Existing geological maps served as a reference (Ambühl 1929; Huber 1943; Mercolli et al. 1994; Berger et al. 2017). Since pre-Mesozoic structures can hardly be investigated by digital elevation models (DEM) or orthophotos, we conducted extensive digital field mapping. By combining newly gathered data with existing reference maps, our geological map was compiled with the software "QGIS". To reach a satisfactory interpretation of the Schlingen structure, we selected all structures that were deformed by the Schlingen phase. From this subset, which contains structural measurements, contact lines and foliation trajectories, we reproduced the gross geometry and axial trace of the central Tros Schlinge. The same procedure was applied for the interpretation of axial planes on the superimposed Vermigel phase (see below). The spatio-temporal relationships between different foliations and their distinctive petrological and textural features were determined by macroscopic hand specimen investigations and thin section microscopy. We applied this approach to roughly estimate the metamorphic conditions for the different deformation phases. The distinction of the mapped lithologies is based on macroscopic textural and petrographic characteristics, following hand specimen observations and modal compositions determined from microscopic thin section evaluation.

Geochronology—LA-ICP-MS U/Pb dating

To constrain an age for the Schlingen phase, we sampled leucosomes at the Tros location that formed parallel to the axial plane of the kilometre-scale Tros Schlinge. Sample preparation was done at the Institute of Geological Sciences, University of Bern. Samples were disaggregated using a SelFrag Lab system by high-voltage discharge and sieved to a grain size of 63–580 µm. Zircons were separated by using conventional magnetic and heavy liquid techniques. The hand-picked grains were analysed based on charge contrast (CC) and backscattered electron (BSE) imaging with a ZEISS EVO 50 electron microscope (see operating conditions in Appendix B). It has been previously demonstrated that CC images correlate exactly to cathodoluminescence (Watt et al. 2000), as also confirmed by checks in the Bern laboratory.

A total of 98 U–Th–Pb analyses were performed on zircon rims and cores using a RESOlution Laser System SE, ATL Laser head and an Agilent 7900, Q-ICP-MS instrument at the Institute of Geology Geological Sciences, University of Bern. Analytical conditions and run table are reported in Appendix B. Different reference materials were used to correct laser-induced elemental fractionation and instrumental mass bias and to monitor the precision and accuracy of the analyses. The TEM2 zircon (Black et al. 2003) served as a primary reference material and zircon Plesovice (Sláma et al. 2008) and 91,500 (Wiedenbeck et al. 2004) as secondary reference materials (see Appendix B for details). Subsequently, data were processed in the software IOLITE (Paton et al. 2011) and data reduction was accomplished according to Petrus and Kamber (2012). All errors are stated at the 2σ-level and propagation is calculated by quadratic addition after Horstwood et al. (2003). Data visualisation

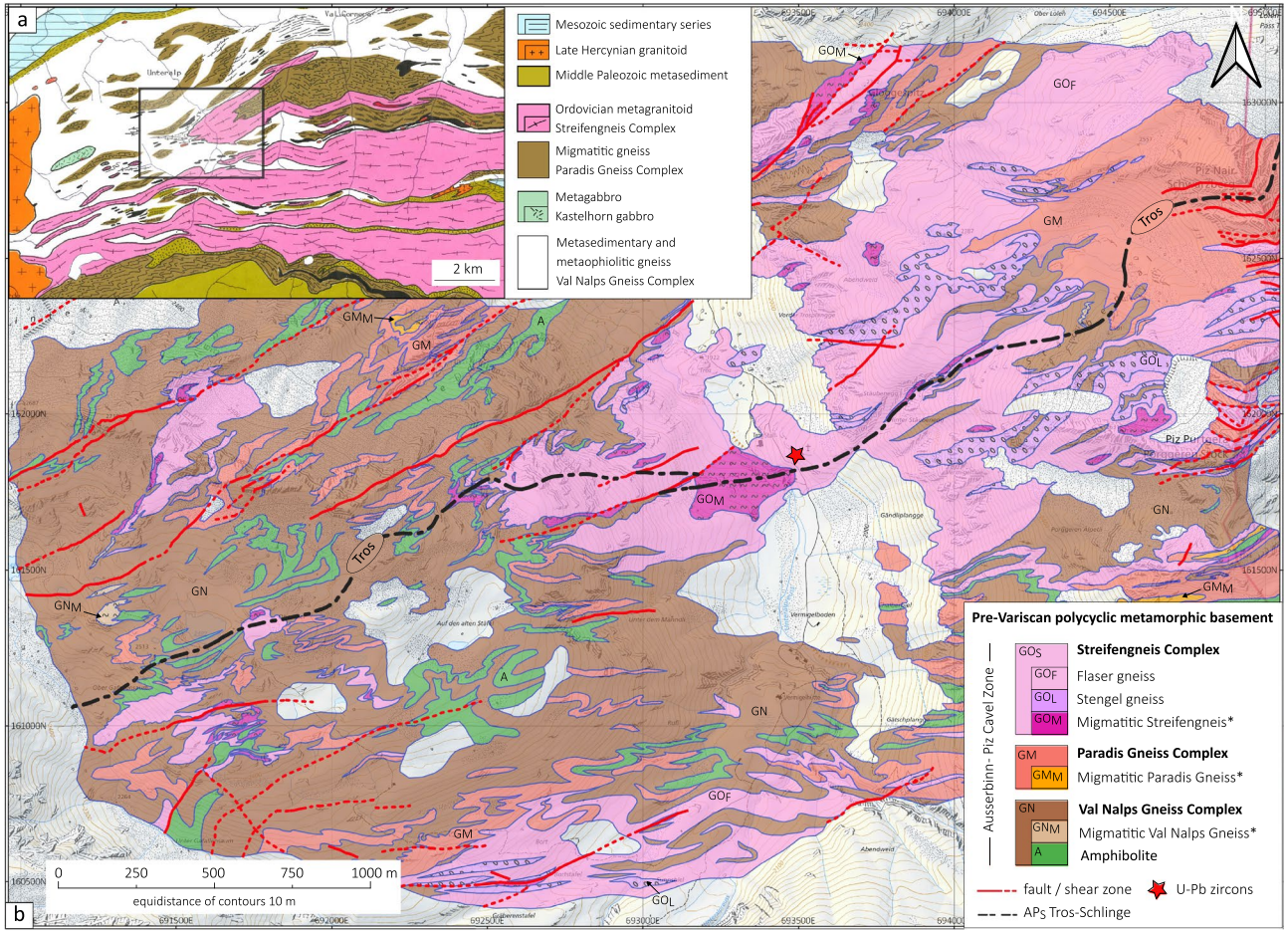

Fig. 2 Geological map of the central Gotthard nappe. **a** Compilation map of the central Gotthard nappe (Mercolli et al. 1994). Black rectangle indicates the study area. **b** Geological map of the Unteralp Valley. *Migmatites associated with the Schlingen phase

Unit	Characteristic rock types and local names	Compilation Map: Mercolli et al. 1994		Compilation Map: Berger et al. 2017		This Study		
γb	basic dykes; lamprophyre	no MMU (minimum mapping unit)		mapped		metabasic dyke		
γLe	saure und intermediäre Gänge	no MMU		mapped		leucocratic dyke		
GO_S	Streifengneis, two -mica gneiss, Orthogneis, Granitgneis, Stengelgneis, Augengneis	late Ordovician metagranitoids	Proto Gotthard; pre late Ordovician	Streifengneis Complex	Ausserbinn – Piz Cavel Zone	Streifengneis	flaser gneiss GO_F	Pre-Mesozoic polycyclic metamorphic basement
							stengel gneiss GO_L	
							migmatitic Streifengneis* GO_M	
GM	Paradisgneis, Schmitzengneis, mica-plagioclase gneiss rich in inclusions	migmatitic gneisses (diatexite)		Paradis Gneiss Complex		Paradis Gneiss		
	(homogene) Mischgneise, chorismatische Gneise, Injektionsgneise, feldspatreiche Gneise, Migmatitgneise						migmatitic Paradis Gneiss* GM_M	
GN	nördliche Paragneise, Glimmer-Plagioklas-Gneise	metasedimentary gneisses		Val Nalps Gneiss Complex		Val Nalps Gneiss	garnet amphibole biotite gneiss	
	Metagabbro, Serpentinit, Talkschiefer, Kalksilikatfefls	metagabbro, metabasalts and metaultramafics with ophiolitic affinity					granitic, gabbroid, ultramafic lenses and calcsilicate nodules	
							migmatitic Val Nalps Gneiss* GN_M	
A	Amphibolite						amphibolite	

Fig. 3 Main lithologies of the presented geological map for the Unteralp Valley. Correlation of pre-Mesozoic units described by a selection of studies for the Gotthard nappe. Local names refer to Ambühl (1929) and Huber (1943). Common lithologies of the Gotthard nappe such as late Carboniferous granitoids as well as sediments of the Val Rondadura group (Berger et al. 2017) do not appear in the study area

in Concordia diagram, age density plots as well as weighted mean ages were performed in Isoplot 3.75 (Ludwig 2012). No correction was applied for common Pb. Average ages were forced to at least 1% to account of external accuracy.

Field results

Lithological observations

The gneiss complexes of the Val Nalps and Paradis constitute the country rocks of the Streifengneis (Fig. 2). Metasedimentary gneisses of the Val Nalps Gneiss Complex are the most abundant unit (Berger et al. 2017, www.strati.ch). The alternating sequences contain coarser-grained darker garnet, biotite and amphibole-bearing layers and finer-grained quartz and feldspar-rich felsic sequences, pointing to marly-argillaceous and sandy protoliths. The sedimentary origin is further emphasised by contrasting grain sizes that indicate compositional banding owing to sedimentation. The widespread Val Nalps Gneiss shows intercalated banded amphibolites (A in Fig. 2b) that occur most frequently as deformed banded garnetiferous amphibolites in the Val Nalps Gneiss and more rarely within the Paradis Gneiss (see Fig. 2b). Amphibolites could not be observed in the Streifengneis. The amphibolites show a great variation in shape (e.g. bands, layers, lenses and inclusions) and dimensions (from few decimetres up to several decametres thickness).

The Paradis Gneiss Complex is a migmatite that displays different stages of migmatisation and various textures (Fig. 3). The matrix is dominated by quartz and two feldspars and shows a weak solid-state foliation. Some varieties, especially in the central hinge zone of the Tros Schlinge, are

rich in angular inclusions of mica gneisses containing older folded foliations.

The Streifengneis is subdivided in the study according to its texture into three distinctive varieties, namely flaser gneiss, stengel gneiss and migmatitic Streifengneis (Fig. 3). The Streifengneis is a medium- to coarse-grained biotite *K*-feldspar gneiss, occasionally with flakes of muscovite and biotite lathes defining its foliation. In most occurrences, the unit shows a distinctive anastomosing foliation from which the subunit flaser gneiss is derived. Centimetre-sized K-feldspar phenocrysts may occur in the less deformed bands. In addition, locally migmatites crop out as stromatic metatexites that are also deformed. At the mapped scale, leucocratic dykes are numerous (Fig. 4a). They have a predominant magmatic fabric with large euhedral muscovite grains and slightly smaller feldspar grains. Pegmatitic varieties have no pronounced cleavage aside from smaller overprinted bands affected by subgrain rotation recrystallisation (SGR) of quartz and feldspar grains.

In the Unteralp Valley, metabasic dykes are less frequent than aplitic dykes ($n = 20$ in Fig. 4b). They show sharp contacts with the host rocks, indicating rapid emplacement and crystallisation. The presence of centimetre-wide chilled margins and biotite-rich reaction rims in the host rock may be attributed to fast cooling of crystallising dykes. Dykes are from few decimetres to a couple of metres thick and most of them are oriented vertically. Commonly metabasic dykes occur in multiple en-echelon oriented elongated lenses. The mineral assemblage consists of biotite, hornblende, plagioclase, K-feldspar, quartz, epidote and chlorite. Metabasic dykes are only rarely deformed and show a weak N–S trending foliation.

Structural observations

Observed structures in the central Gotthard nappe are assessed and evaluated according to previous studies as summarised in the following. D_X, S_X, AP_X and L_X, refer to deformation event, associated foliation, axial plane and lineation, respectively. The presented kilometre-scale Tros Schlinge is associated with its eponymous Schlingen phase D_S and deforms older structures belonging to the Tuma (D_T) and the Ravetsch (D_R) phases (Table 1).

Primary foliations S_0

Slightly discordant decametric inclusions spotted in the Val Nalps Gneiss contain rhythmic alternations of feldspar and mica-rich sequences. This compositional banding might represent a relict of sedimentary bedding (Fig. 3a and b).

Tuma phase D_T

Only few relic structures of this deformation event are preserved in the investigated area, because subsequent strong overprinting during later-staged deformation has obliterated D_T features. Still, large, resorbed garnet porphyroblasts with pressure shadows filled with felsic minerals signal a post-migmatitic deformation under garnet amphibolite-facies conditions prior to the intrusion of the protolith of the Streifengneis (Fig. 5c). Furthermore, the Paradis Gneiss and Val Nalps Gneiss contain strongly elongated gneissic inclusions with an internally deformed S_T foliation (Fig. 5a) marked by newly grown biotite. The S_T is interpreted as a pre-intrusive foliation. Present-day orientations of foliation planes S_T and fold axes are steep and do not deviate significantly from superimposed deformation structures. Most preserved structures are composite S_0 and S_R foliations.

Ravetsch phase D_R

The Ravetsch phase accounts for the most pronounced foliation in the study area and is associated with the metamorphic overprint of the protolith of the Streifengneis (Table 1). The D_R structures include subvertical, close to isoclinal folds ranging from millimetres to several metres in size. Fold interference between D_T and D_R is observed in banded varieties of Val Nalps Gneiss with tightly folded leucosomes parallel to S_R foliation planes. The type of S_R foliation varies due to different rheologies and contrasting grain sizes. Within sequences of finer-grained varieties of the Val Nalps Gneiss, we observed a continuous, penetrative foliation marked by brown biotite, whereas coarser-grained varieties show a wide-spaced and partly anastomosing foliation with microlithons consisting of recrystallised feldspars, quartz, minor muscovite and bordering biotite. The foliation spacing decreases according to grain size, which is also linked to the geometrical position within the Schlingen fold. For instance, in fold limbs lithological contacts show a dramatic decrease of grain size and foliation spacing. Feldspar and quartz porphyroclasts are recrystallised by SGR and show minor undulous extinction. White mica, biotite and the rim of garnet poikiloblasts and new garnet in the matrix grew syn-kinematically with S_R. In amphibole-bearing gneisses as well as amphibolites, biotite overgrows amphibole porphyroblasts during S_R development. The mineral assemblage comprising garnet, hornblende and biotite indicates amphibolite-facies conditions.

The S_R orientation is characterised by moderate to subvertical dips of 60°–90° (mean of 76°) with an average dip azimuth of 336° ($n = 1444$) mirroring the general strike of the Gotthard nappe (Figs. 5a and 6a). The scattering of S_R is due to the reorientation effects by younger deformation phases, mostly attributed to the Schlingen phase (Fig. 6a,

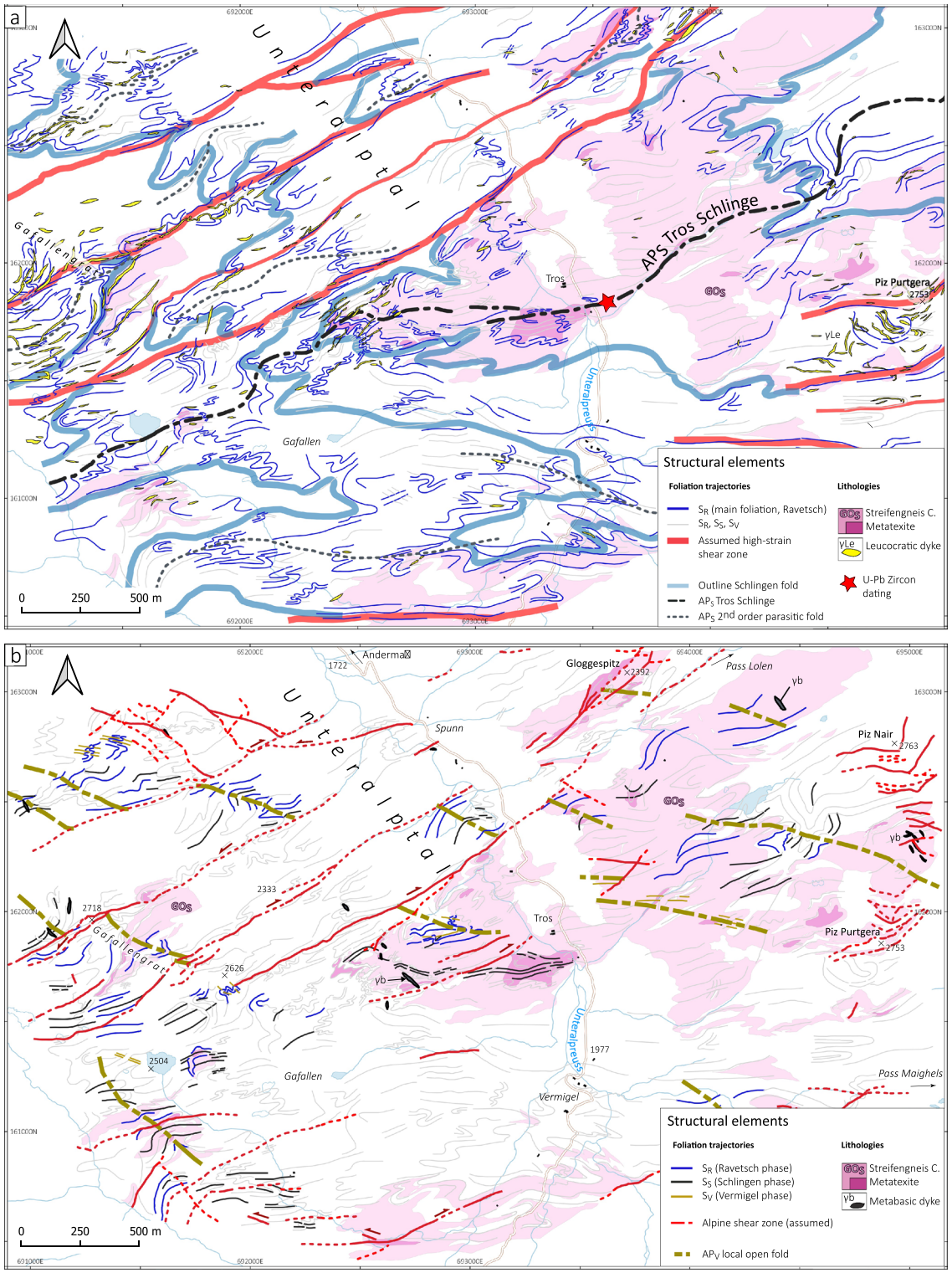

Fig. 4 Structural maps: **a** Schlingen phase: foliation trajectory map of structures associated with the Schlingen phase D_S. **b** Vermigel phase: foliation trajectory map of structures associated with the Vermigel phase D_V

see next section). L_R lineation is steep and either marked by centimetre-long feldspars or by the shape preferred orientation of hornblende in amphibolites or hornblende bearing varieties of Val Nalps Gneiss. The plunge of L_R ranges from 60° to 90°. The trend scatters along foliation planes dipping mostly towards SW with an average orientation of 249/76 ($n = 62$). The contact between the Streifengneis body and its host rock is slightly discordant (10°) with a subparallel S_R foliation.

The emplacement of the of the Streifengneis granitoid produced contact migmatites in the host rock (Val Nalps Gneiss), which are commonly associated with leucocratic dyke swarms (GO_M in Fig. 2b and GO_M and γ_{Le} in Fig. 4a). Some of the aplitic dykes in the vicinity of the Streifengneis body are folded, for instance around Piz Purtgera and east of Gafallen (Fig. 4a). In contrast to axial plane parallel leucocratic dykes associated with the Schlingen phase, the Ravetsch dykes are thicker (0.5–20 m) and longer (10–500 m). Leucocratic dykes of the Schlingen phase are steeply inclined and strike slightly discordant (10°) to the S_R foliation (Fig. 6c). In rare cases, leucocratic dykes contain a foliation.

Schlingen phase D_S

The Schlingen deformation phase D_S profoundly influenced previous structural patterns, in particular the S_R foliation. It is accountable for NE- to SW-verging isoclinal folds (Fig. 4a). Mapped Schlingen folds are moderately to very tight, with inter-limb angles around 30° for

Table 1 Correlation of deformation phases in the Gotthard nappe. Alpine phases are briefly summarised and are not the focus of this research

	Name	Ref. text	Literature	Short description	This study
Alpine	**Alpine phases** Chiera phase Domleschg phase Ferrera phase	D_A	· Pfiffner 2014 · Wiederkehr et al. 2008, 2009 · Pettke and Klaper 1992 · Klaper 1985	· Northern Steep Belt (NSB) folding and crenulation of Alpine foliations · Pennine nappe refolding, accretion of cont. basements · Decompression, Alpine thrusting	· Foliation fanning of S_R as proposed by Heim 1891, Marquer 1990, Zangerl et al. 2006, Labhart and Renner 2012 · Brittle ductile shear zones · Steep reverse faulting (S-top), pure shear dominated subvertical shear zones with sinistral (E-W) or dextral (NE-SW) offset
Pre-Alpine	**Vermigel phase**	D_V	previously not reported		Local open folds, decameter half-wavelength, sparsely occurring, locally weak foliation
	Schlingen phase	D_S	Schlingen phase (D3) · Zurbriggen et al. 1998 · Van Gool et al. 1987	Schlingen folds	· Folding: Steep kilometer-scale folds · Melting: migmatisation in fold hinge of Schlingen folds · High-strain mylonitic shear zones
	Rondadura phase*	D_{Ro}	Steiger 1962	Deformed foliation of metasediments of the Rondadura phase	D_S deformed foliation of metasediments of the Val Rondadura Group
	Ravetsch phase	D_{R2}	D2 · Huber 1943 · Mercolli et al. 1994	Predominant foliation, Syn-intrusive overprint of Streifengneis C.	· Steep structures · Metamorphic overprint of all major units · Migmatisation in contact zones · folding
		D_{R1}	previously not reported		· Local, folded foliation in metatexites of Streifengneis · Stromatic · Fine-grained bands
	Tuma phase	D_T	(D1) · Niggli 1944 · Huber 1943	Pre- Streifengneis foliation	Deformed foliation in angular or lenticular shaped inclusions in GM and GN units.
		S_0	Bedding planes · Niggli 1944 · Arnold 1972	Sedimentation of pelite-greywacke and arkose series with intercalated calcareous layers	· Compositional banding

*Outcrops of structures and rocks associated with the Rondadura phase are southwards of the study area

first-order and second-order parasitic folds. Schlingen have a fractal character which is expressed on the microscale by S_R crenulation cleavage or isoclinal microfolds and in the map scale represented by the folded Streifengneis with an amplitude of up to several kilometres (Figs. 2a). The foliation trajectory map displays only the fold hinge of the kilometre-scale Tros Schlinge (AP_S) with a half-wavelength of ~ 2800 m and several second-order parasitic folds with wavelengths of approximately 500 m (AP_S in Figs. 2b and 4a). It is interesting to note that most Schlingen folds close southwest and corresponding northeast closing folds are missing. Both symmetric and asymmetric lower-order folds have been identified depending on their position within the fold geometry (M-type versus S- and Z-type parasitic folds). Our results confirm that the gross geometry of the Tros Schlinge affects the central Streifengneis body (Fig. 2a and b). The Schlingen phase also deforms the surrounding Val Nalps Gneiss and Paradis Gneiss and creates intense folding of more competent thinner gneissic sheets. Foliation structures related to the Schlingen phase are visible in hinge areas of map-scale Schlingen folds, owing to their oblique nature to older foliations. The S_S is a subvertical (60°–90°) axial planar foliation that strikes NE–SW, with an average orientation of 327/75 (Fig. 6b). A composite foliation of S_R and S_S is observed along the fold limb. Fold axes of the Tros Schlinge in parasitic folds (FA_S) as well as axial planes (AP_S) are steep with an average orientation of 252/70 and 329/85, respectively (Fig. 6a). Similar to the Ravetsch phase, L_S are marked by elongated feldspars and amphiboles with a subvertical plunge, however, slightly less steep than the L_R (L_S: 276/68, $n = 29$; L_R: 249/76, $n = 62$). The folding style varies according to the geometrical position within the Tros Schlinge, the rheology of adjoining rock units and original grain size variability of the host rocks (Fig. 7a and b). For instance, ptygmatic folds in the Streifengneis and the Val Nalps Gneiss likely resulted from shortening of more competent felsic layers than the enclosing rock. A few sheath folds are observed in metatexites in the Streifengneis or high-strain shear zones indicating intense folding and shearing. The S_R foliation is strongly crenulated by S_S showing millimetre- to centimetre-scale (micro) folding (Fig. 7b and d). The prominent and widespread S_S foliation has spacing varying from 0.5 to 20 mm. Crenulation lineations are nearly subvertical and scatter considerably in the fold limb. Recrystallisation of mica occurs in the inner cores of lower-order Schlingen fold hinges, where biotite defines an axial plane foliation (Fig. 7e and f). Moreover, in garnet- and amphibole-bearing gneisses and amphibolites, euhedral garnet porphyroblasts and subhedral amphiboles are found syn- to post-kinematically with respect to S_S. The mineral assemblage associated with the Schlingen phase comprises garnet, biotite and amphibole indicating amphibolite-facies metamorphism.

In the migmatitic Streifengneis, a variety of leucosome types is observed (Fig. 7d, e, f): (i) small, crenulated fine-grained leucosome Le_A, frequently bordered by biotite selvages, was formed concordant to the S_r; (ii) patchy, irregular and discontinuous leucosomes Le_B had well-developed melanocratic selvages; (iii) coarse-grained leucocratic dykes Le_C had rather diffuse margins, displaced type Le_A leucosomes and showed interconnected asymmetric pinch-and-swell structures that were slightly discordant to the S_S foliation of the metatexites.

An additional structural feature indicative of the Schlingen phase is the presence of high-strain shear zones that are 20–50 m wide. Densely spaced and perfectly parallel foliation bands are a repetitive element between NE- or SW-verging Schlingen folds (Fig. 4a). Such high-strain zones are characterised by a parallelised, locally anastomosing and mylonitic subvertical foliation. Internal shear bands of 1-m width show a grain size reduction. Additionally, leucocratic polymineralic dykes become more frequent within such high-strain shear zones (Fig. 4a) and show pinch-and-swell structures. The shear zones occasionally contain folded and sheared metatexites and field observations suggest that partial melting was synchronous to shearing. Structural data of composite S_R and S_S foliation and corresponding L_R and L_S lineation indicate two sets of ductile shear zones. An E–W striking set with an average orientation of 003/73 is most prevalent towards the northern and especially southern border of the Tros Schlinge around the Vermigel and Maighels pass (Fig. 4a). In between, the prevalent NE–SW striking set is virtually parallel to the axial plane of the Tros Schlinge with an average orientation of 150/76. Corresponding lineations plunge towards SW. Sigmoidal boudins indicate an oblique south block-up movement with a slight dextral component for the NE–SW striking set. Such polymineralic boudins are particularly frequent in high-strain zones and indicate a steep reverse movement (see below).

Vermigel phase D_V

The axial trace of the Tros Schlinge, together with the corresponding AP_S of second-order parasitic folds, is slightly wavy (Figs. 2b and 4a). This local, small undulation is attributed to a superimposed minor deformation event D_V, which we name the Vermigel phase (Table 1). Moreover, in contrast to Schlingen-related folds, Vermigel folds show a significantly smaller half-wavelength (~ 150 m). A weak foliation (S_V in Fig. 4b) has a steep orientation with a WNW–ESE strike oblique to the axial trace of the Schlingen folds (Fig. 6b). Reconstructed axial planes are steeply inclined and locally deform Schlingen-related structures

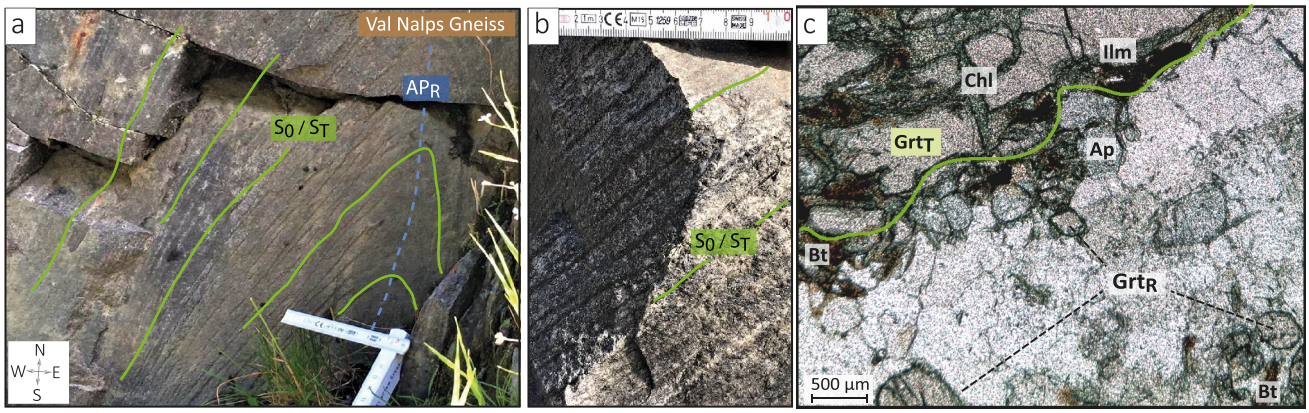

Fig. 5 Field aspects of the Tuma D_T and the Ravetsch D_R phases. **a** Deformed composite foliation/banding (S_0, S_T) in fine-grained inclusions of the Val Nalps Gneiss (2,692,528/1,162,842). **b** Detailed view of compositional banding. **c** Fractured and resorbed garnet poikiloblasts (Grt_T 1.5 cm) with felsic pressure shadows in an inclusion associated with the Tuma phase. New euhedral garnets Grt_R of the Ravetsch phase grow in the vicinity of larger garnet poikiloblasts (2,692,535/1,162,842). All coordinates are in CH1903+ / LV95

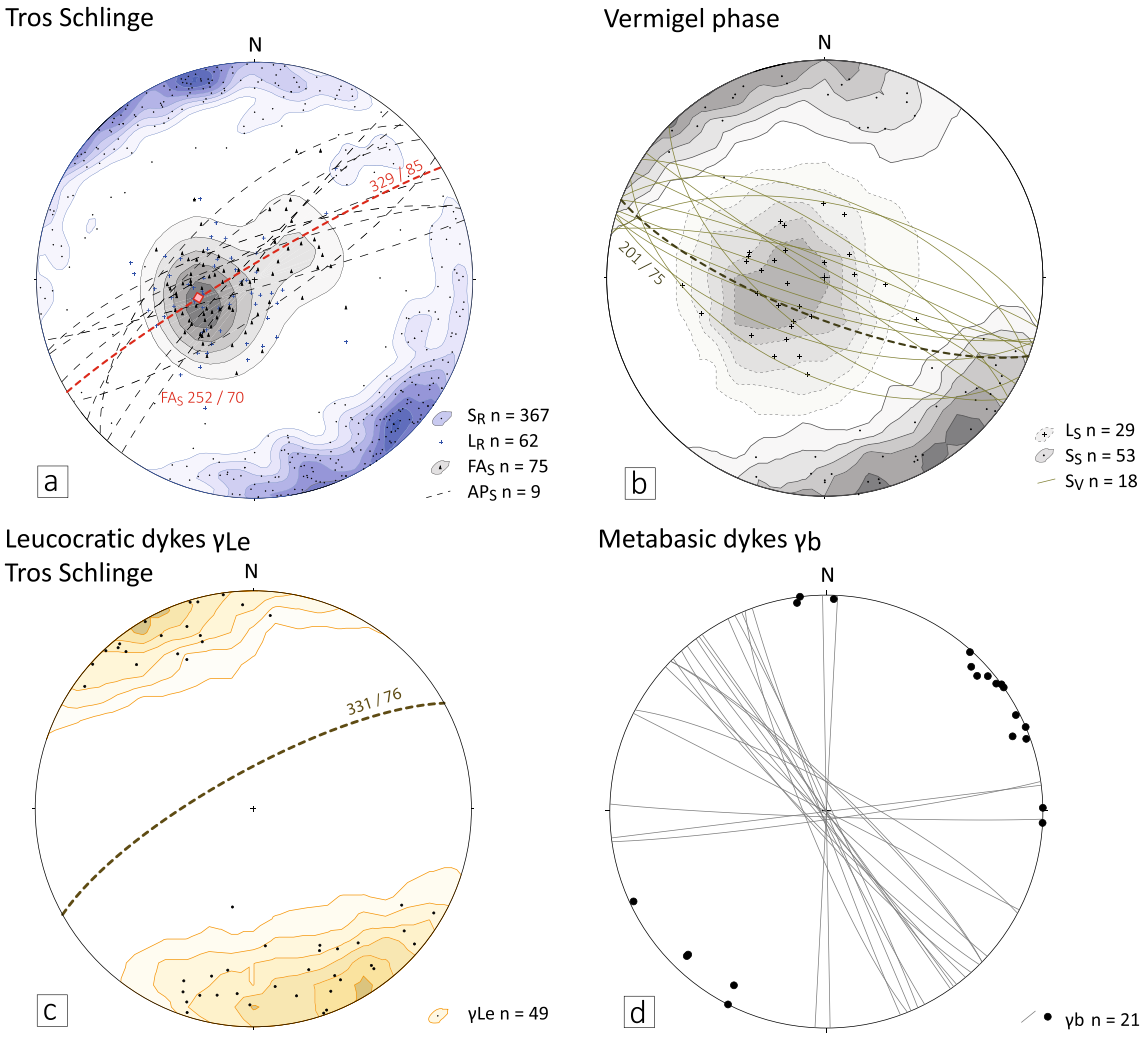

Fig. 6 Stereoplots (equal area, lower hemisphere) of structural data from the study area showing a dominant NE–SW orientation. Stereoplots for **a** D_R and D_S structures for the Tros Schlinge; **b** Vermigel phase, whole study area; **c** leucocratic dykes associated with the Tros Schlinge; **d** metabasic dykes, whole study area. *n* number of measurements, *S* foliation plane, *FA* fold axis, *AP* axial plane, *L* lineation, subscripts *R*, *S*, *V* indicate corresponding deformation phases, see Table 1

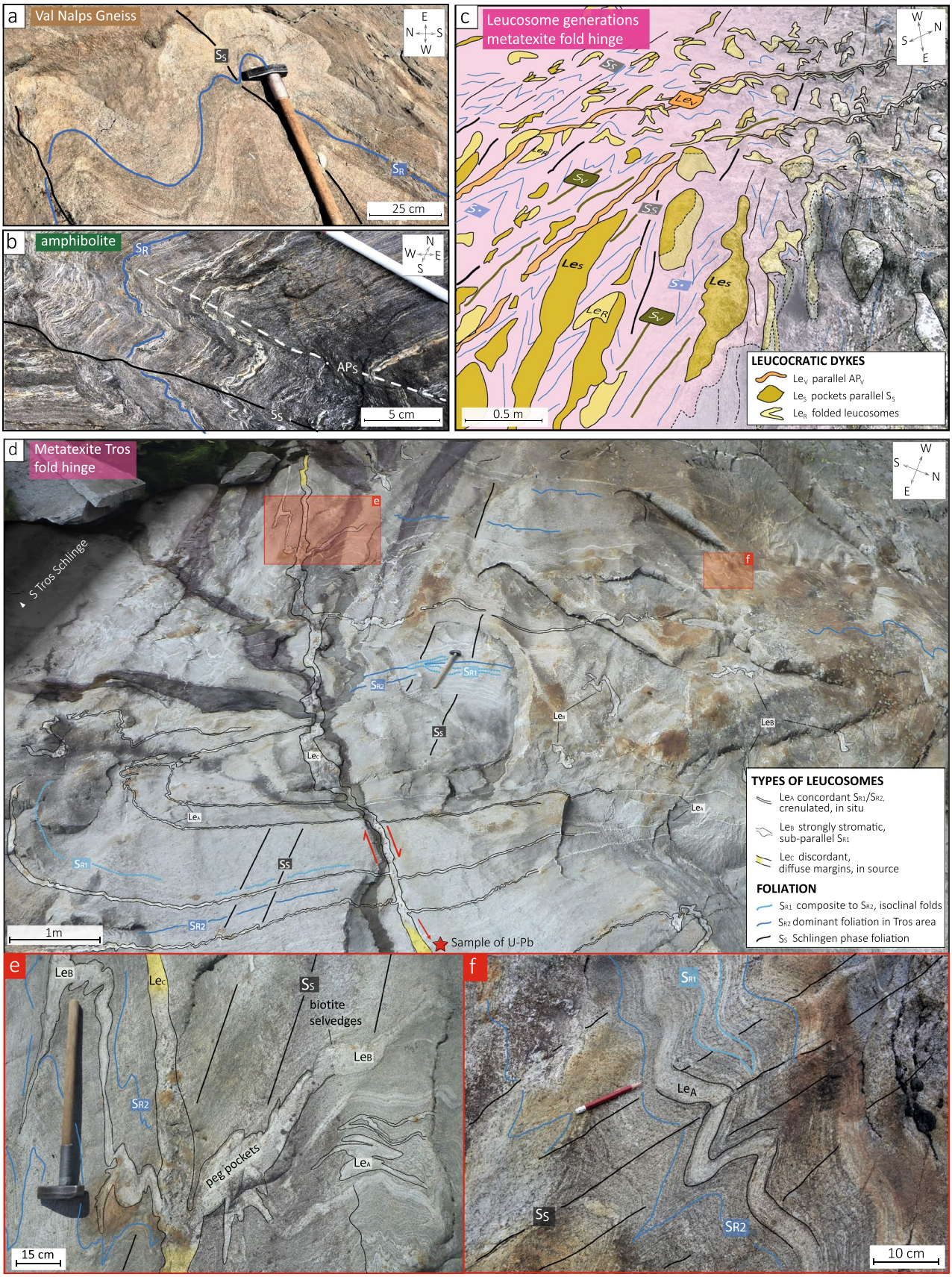
a
Val Nalps Gneiss
E
N
S
W
Ss
SR
25 cm
b
amphibolite
SR
N
W
E
S
APs
Ss
5 cm
c
Leucosome generations
metatexite fold hinge
W
N
S
E
Ss
LeV
LeR
Sv
Les
0.5 m
LEUCOCRATIC DYKES
LeV parallel APV
LeS pockets parallel SS
LeR folded leucosomes
d
Metatexite Tros
fold hinge
W
S
N
E
e
f
S Tros Schlinge
SR1
SR2
Ss
LeB
LeC
LeA
1m
Sample of U-Pb
TYPES OF LEUCOSOMES
LeA concordant SR1/SR2, crenulated, in situ
LeB strongly stromatic, sub-parallel SR1
LeC discordant, diffuse margins, in source
FOLIATION
SR1 composite to SR2, isoclinal folds
SR2 dominant foliation in Tros area
Ss Schlingen phase foliation
e
LeB
LeC
Ss
biotite
selvedges
LeB
SR2
peg pockets
LeA
15 cm
f
SR1
LeA
Ss
SR2
10 cm

◂**Fig. 7** Structural relationships of the Ravetsch and the Schlingen phase. **a** Folded banded Val Nalps Gneiss (2,691,205/1,161,530). **b** Crenulated and folded banded amphibolite (2,691,861/1,161,458). **c** Relationship between different types of foliations and corresponding leucosomes in the fold limb of the Tros Schlinge. The Vermigel foliation marks the youngest stage and strikes NW–SE (2,692,848/1,161,878). **d** Structural features of the Tros outcrop in the fold hinge. Two generations of migmatisation are indicated by deformed foliation S_{R1} and S_{R2} and corresponding leucosome generations. The Schlingen related foliation S_S strikes here ENE–WSW (353/88) and is subparallel to the youngest leucocratic dyke (Le_C: 330/86; 2,693,407/1,161,796). **e** Phenomenological progression of leucosomes from in situ well-evolved leucosomes (Le_A), to discordant pegmatitic pockets (Le_B). The leucocratic dyke Le_C marks the final stage and is subparallel to the axial plane of the Tros Schlinge. It dissects the Schlingen foliation S_S. **f** The only locally observed S_{R1} foliation is tightly folded by dominant S_{R2} foliation. Both foliations strike NNW–SSE in the Tros outcrop

(AP_V: 201/75). In the fold hinge of the central Streifengneis body 550 m northwest of the Tros outcrop, leucocratic dykes are parallel to a poorly developed biotite and muscovite containing spaced foliation, presumably accounting for the Vermigel phase (Fig. 7c). S_V microstructural investigation revealed a realignment of predominantly muscovite, chlorite and few biotite flakes. Biotite retrogression and occurrence of chlorite suggests greenschist facies metamorphic conditions slightly below 400 °C.

Interestingly, D_S structures are dissected by metabasic dykes (γ_b in Fig. 4b) that intruded en-echelon vertically into pre-existing basements units and are spread over the whole mapping area (Figs. 4b and 6d). Metabasic dykes have a fine-grained isotropic texture with chilled margins. A minority of dykes, in particular, in between Piz Purtgera and Piz Nair, contain a weak NNW–SSE trending vertically dipping foliation. The dykes have mostly a NW–SE elongation, which is subparallel to the Vermigel foliation (Fig. 6b and d). As overprinting relationships are lacking, the dike emplacement could not be unambiguously attributed to either Vermigel or younger deformation phases.

Alpine deformation D_A

The investigated field area was affected by Alpine deformation only locally and to a minor extent. In detail, the previously discussed high-strain shear zones related to Schlingen are rarely overprinted by small discrete brittle–ductile shear bands that are presumably remnants of Alpine deformation. A first set of shear zones has an oblique dextral component with an average orientation of 146/73. These NE–SW striking brittle–ductile shear zones reveal a regular spacing of roughly 300 m (Fig. 4b). Some of them extend over several kilometres and displace the axial planes of the Vermigel phase as well as the Schlingen structures (Figs. 2b and 4). A second set has an E–W orientation (359/78) similar to the high-strained gneissic sequences (Fig. 4b). Corresponding shear zones are most prominent in the east and south of the mapped area and may represent Alpine shear zones reactivating older pre-existing ones. Most veins in the vicinity of these shear zones show quartz and chlorite pockets, which are typical for Alpine overprint and fluid–rock interaction at greenschist–facies conditions. Some of the brittle–ductile structures are overprinted by cohesive, random-fabric, crush breccias and cataclasites. Abrupt contacts between faulted rock (gouge and fault breccia) and undeformed host rock as well as calcite and quartz clasts are typical. The width varies from discrete brittle fault zones of 20–50 cm to millimetre-thick phyllosilicate bands. All these observations indicate again subsequent deformation under progressively cooling temperatures, which is typically the case during Alpine exhumation.

Zircon chronology

To resolve the age relationship between the Schlingen phase and the preceding Ravetsch phase, we performed U–Pb zircon dating of one leucosome that formed parallel to the AP_S in close proximity eastwards of the Tros metatexite (Figs. 2b and 4a). In the area, the Ravetsch foliation S_R is heavily deformed and forms M-type lower-order parasitic folds, which are dissected by an axial plane foliation (AP_S, S_S) and coarse-grained leucosomes (Fig. 8a). The leucosome consists mainly of quartz, K-feldspar, albite and muscovite. Microscopically, the investigated sample has a granoblastic decussate texture (Fig. 8b). Quartz is polycrystalline and plagioclase is locally replaced by sericite. Dynamic recrystallisation by subgrain rotation (SGR) and bulging is observed in some feldspar and quartz grains. Few K-feldspar grains show perthitic exsolution textures. Generally, pristine crystalline texture is well preserved in the leucosomes and post-crystallisation overprinting relationships do not establish a new penetrative fabric. The magmatic texture is only affected by minor solid-state grain size reduction of quartz and feldspars.

Zircon grains separated from leucosome LEU9 are prismatic to nearly euhedral (Figs. 9a–c). While smaller grains are transparent, larger grains (150–310 µm) appear brown with a rusty colour, likely due to metamictisation. The CC images exhibit complex internal zircon textures with various core and rim generations. Most grains contain a variably zoned core that is truncated by a low luminescent rim (Fig. 9a–c). The oscillatory and planar zoned cores (C2) are present in virtually every grain; they have moderate U and Th contents and relatively high Th/U ratio around 0.02–1 (Fig. 9e and f, supplementary Table). Some analysed grains have a complex xenocrystic core indicating a pre-magmatic inheritance (e.g. C1 in zircons B17 and B51 in Fig. 9a and b, respectively). Mineral inclusions in zircon are K-feldspar,

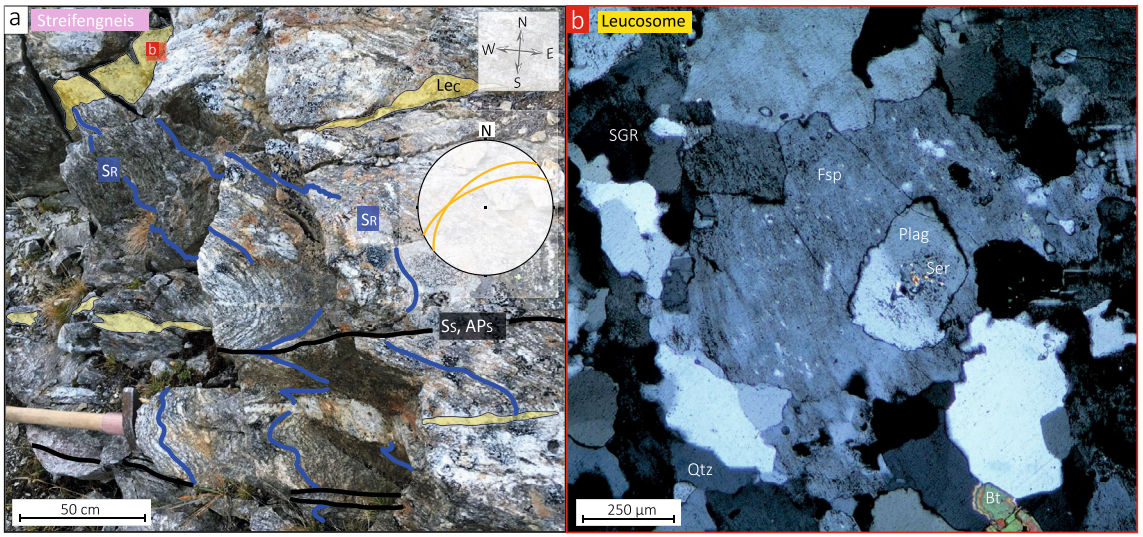

Fig. 8 Axial parallel leucosome $Le_{C,}$ (Leu9) that was sampled for isotopic dating. **a** Field image of crosscutting relationship between elongated leucosomes and foliation planes S_R and S_S (2,693,458/1,161,856). Exact location of leucosome (Le_C) parallel to AP_S is asterisked in Figs. 2 and 4a. **b** Thin section photomicropgraph of coarse-grained leucosome with two generations of feldspar (Plag core and perthitic rim), and grain size reduction (SGR) of quartz followed by annealing

apatite and quartz and rarely albite, in line with a granitic mineral assemblage.

Of particular interest are the discordant, low luminescent rims that are subdivided into three different types according to texture, composition and age (*R*1, *R*2 and *R*3 in Fig. 9). They generally have euhedral shape, high U content and low Th/U ratio < 0.1 (Fig. 9e and f), comparable to that reported for anatectic zircon (e.g. Rubatto et al. 2009, 2013). Notably, the different types of rims are generally found in different crystals. *R*1 rims grow on euhedral cores, with little or no sign of resorption (Fig. 9c); they have an intermediate Th/U of 0.01–0.1. *R*2 rims are slightly larger than *R*1 and *R*3 rims, and generally cut across the zoning of the resorbed cores. They are the lowest in Th content, with a tight Th/U of 0.006–0.017. *R*3 rims are particularly dark in CC images, with the highest Th and U content and Th/U < 0.3; they appear cloudy and contain more inclusions than *R*2. Furthermore, most *R*1 zircons show a CL-bright very thin outer rim that could not be analysed.

U–Pb analyses reveal two broad major zircon populations (Fig. 9d, Appendix B). Older dates scatter around 450 Ma and younger dates are distributed around 300 Ma, but with a spread from 270 to 330 Ma; Fig. 9d). Most concordant analyses on C1 cores define a cluster with a weighted mean $^{206}Pb/^{238}U$ age of 449.1 ± 2.6 Ma (MSWD = 2.5; *n* = 41). The few analyses on texturally older C2 cores have scattered concordant dates between ~ 570 and 780 Ma.

The *R*1 rims that grow on euhedral cores are Devonian in age. Seven *R*1 analyses define an average $^{206}Pb/^{238}U$ age of 414.1 ± 5.7 Ma (MSWD = 2.0, Fig. 9g). On the other hand, all analyses of *R*2 and *R*3 rims yield Permo-Carboniferous ages. Of the *R*2 analyses, a major cluster returns an age of 315.4 ± 3.7 Ma (MSWD = 3.4; *n* = 13, 2 rejected, Fig. 9g), whereas most analyses on *R*3 define an age of 282.6 ± 3.3 Ma (MSWD = 2.0, *n* = 9, Fig. 9g). In either case, the dispersion of the analyses is slightly above analytical uncertainty and this is not totally unexpected in migmatite samples that underwent protracted or multiple events of melting/metamorphism (e.g. Rubatto et al. 2009, 2013).

Discussion

Timing of magmatism and anatexis

The major zircon fraction with a mean age of 449 ± 3 Ma corresponds to zircon cores that have magmatic oscillatory zoning and composition (e.g. Hoskin and Schaltegger 2003; Corfu et al. 2003), and contain mineral inclusions in agreement with a granitic assemblage (Figs. 9d and g). We interpret the oscillatory zoning as magmatic growth and link the late Ordovician age with the intrusion of the protolith of the Streifengneis, which later underwent anatexis to form the leucosome (see below). Radiometric ages reported in literature for the crystallisation of the Streifengneis are in accordance with our finding (e.g. 436 ± 17 Ma, Arnold 1970; 439 ± 5 Ma, Sergeev and Steiger 1993). Older inherited C1 cores reflect an early Phanerozoic to Proterozoic history. Arnold (1970) argued that the oldest zircon fraction sampled from the Val Nalps Gneiss Complex yields an age of 1.2–1.5 Ga and its associated sedimentation has a younger age limit of 450 Ma.

The nature of the *R*1 rims is not straightforward. They grow concordantly on euhedral magmatic cores, but the generally lower Th/U ratio with respect to the magmatic cores could point to partial melting or metamorphism (e.g. Rubatto et al. 2009, 2013; Rubatto 2017). However, low Th/U ratios have also been described in magmatic zircon (e.g. Lopez-Sanchez et al. 2016). Regarding the age of 414.1 ± 5.7 Ma, two interpretations are plausible from the current state of knowledge: (i) the amphibolite facies metamorphism of the Ravetsch phase was still active; (ii) a hydrothermal event generated the rims ages, related to faulting and uplift of the basement, onto which the sediments of the Val Rondadura Group were deposited subsequently.

The Permo-Carboniferous rims are more clearly discordant on resorbed zircon cores and their low Th/U ratio (< 0.02) is in line with metamorphic overgrowth during high-grade metamorphism and anatexis (Rubatto 2017). Similar zircon rims are commonly found in leucosomes from both ortho- and para-derivates (e.g. Rubatto et al. 2009, 2013). Due to the structural key position of the samples, we associate the melt formation in the hinge of Schlingen folds and its mobilisation along the AP_S with the metamorphic peak of upper amphibolite-facies conditions during Schlingen folding. Thus, we attribute the most prominent zircon fraction (*R*2) dated at 315.4 ± 3.7 Ma to the metamorphic peak of the Schlingen phase (Table 1). Other Schlingen are dated in a similar structural context in the Strona-Ceneri Zone (Zurbriggen et al. 1998), where synkinematic leucotonalitic dykes contain garnet dated at 321.3 ± 2.3 Ma. A late Carboniferous metamorphic event has been dated or inferred in other localities. Dated leucosomes in the Aiguilles Rouges Massif yield an age of ~ 320 Ma (Bussy et al. 2000). In the Belledonne Massif, high-grade metamorphism and migmatisation are constrained between ~ 335 and 305 Ma (Jacob et al. 2021).

The most external zircon rim dated at 282.6 ± 3.3 Ma has comparable textural features to the late Carboniferous *R*2 rims, with equally low Th/U ratios, but even higher U and Th contents (up to 12,000 ppm U). Given the incompatible nature of these elements, it is speculated that R3 rims formed by low degree melting or crystallisation of residual melts enriched in Th and U. It is indeed common that migmatites contain multiple zircon overgrowths that formed during subsequent events of high-grade metamorphism or repeated anatexis (e.g. Rubatto et al. 2009, 2013; Jacob et al. 2021).

Structural evolution

In the crystalline basement of the central Gotthard nappe, the Alpine deformation (D_A) is subordinate compared to the penetrative pre-Alpine Tuma (D_T), Ravetsch (D_R) and Schlingen (D_S) deformation events. Our results confirm that Alpine deformation localises in a few discrete Alpine shear zones (see also Ambühl 1929; Niggli 1944; Marquer 1990; Lützenkirchen 2002; Rast et al. 2022). The Schlingen phase is accountable for the large-scale (sub-)vertical folds that deform the main Ravetsch foliation (S_R). Corresponding Schlingen fabrics are present as a crenulation cleavage or as an axial plane foliation. Field observation allows us to define a relative sequence that we ascribe to different deformation phases (Table 1). Nevertheless, associated mineral assemblages of phase-corresponding foliations and composite foliations underscore how difficult it is to differentiate between different deformation phases, particularly when these are coplanar and of composite nature. In this context, it is important to underline that the pre-Mesozoic basement units are likely to have experienced three times amphibolite-facies metamorphism, namely during the Tuma (Tuma phase D_T), Ravetsch (Ravetsch phase D_R) and Schlingen phases (Schlingen phase D_S). In the following, four main stages of structural evolution of the area are discussed.

(1) Formation of the country rock gneisses. Inclusions containing a deformed S_T foliation are only observed in the Paradis Gneiss and Val Nalps Gneiss. For the Tuma phase, newly grown biotite in S_T as well as resorbed garnet porphyroblasts with felsic mineral precipitation in pressure shadows signal a post-migmatitic deformation under garnet amphibolite-facies conditions prior to the intrusion of the protolith of the Streifengneis (Fig. 3). Thus, we conclude that partial melting is associated with anatexis of the Val Nalps Gneiss and formation of Paradis Gneiss migmatites, suggesting a coeval Ordovician metamorphic evolution (Berger et al. 2017). Regarding the controversially debated formation of the migmatitic gneisses (Paradis Gneiss), our field observations support previous interpretations that (i) they are sedimentary derived, and that (ii) they were affected by subsequent multiple stages of metamorphism and anatexis producing gneissic and migmatitic structures. Hence, the Paradis Gneiss records multiple melting events that, at least in part, preceded the last episode of Schlingen folding and presumably also the Ravetsch phase. However, the youngest migmatitic pulses are associated with high-strain shear zones and the Schlingen phase (GM_M in Fig. 2b).

(2) Intrusion of the protolith of the Streifengneis is dated at 449 ± 3 Ma (Fig. 9a and g, Zircon chronology) and its emplacement is considered syntectonic at amphibolite-facies conditions (see Geological setting and Huber 1943; Niggli 1944). This synemplacement deformation is also recorded in the hosting Val Nalps complex (Mercolli et al. 1994). The kilometre-long steeply inclined sheets of orthogneisses with high aspect ratio reinforce a syntectonic emplacement (e.g. Zurbriggen 2015). Their elongated geometry resulted from transpres-

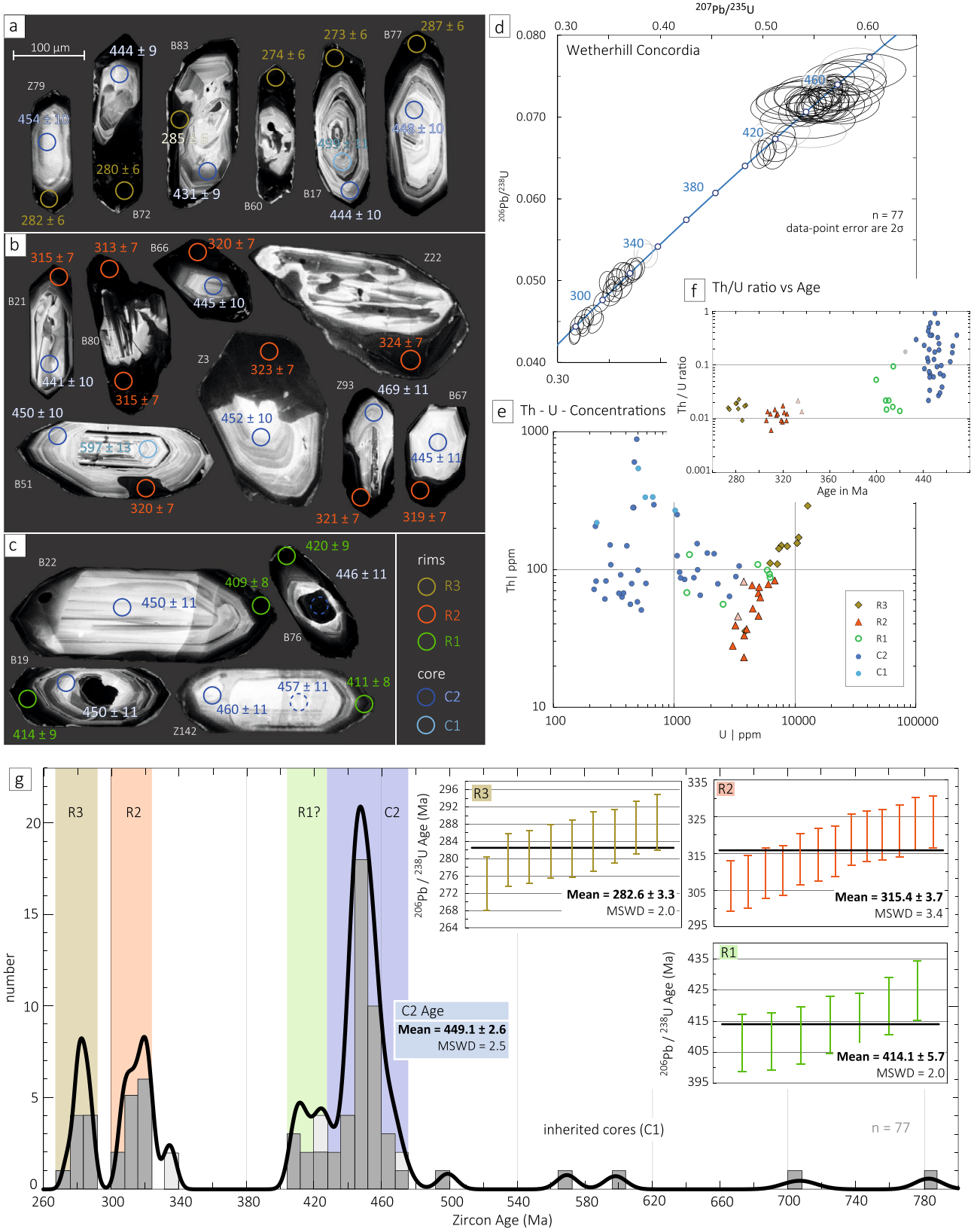
a
100 µm
Z79
454 ± 10
282 ± 6
444 ± 9
280 ± 6
B72
B83
285 ± 6
431 ± 9
274 ± 6
B60
273 ± 6
B17
499 ± 11
444 ± 10
B77
287 ± 6
448 ± 10
b
315 ± 7
B21
441 ± 10
313 ± 7
B80
315 ± 7
B66
320 ± 7
445 ± 10
Z3
323 ± 7
452 ± 10
Z22
324 ± 7
Z93
469 ± 11
321 ± 7
B67
445 ± 11
319 ± 7
450 ± 10
B51
597 ± 13
320 ± 7
c
B22
420 ± 9
409 ± 8
450 ± 11
446 ± 11
B76
B19
450 ± 11
414 ± 9
457 ± 11
460 ± 11
411 ± 8
Z142
rims
R3
R2
R1
core
C2
C1
d
Wetherhill Concordia
207Pb/235U
206Pb/238U
n = 77
data-point error are 2σ
e
Th - U - Concentrations
Th | ppm
U | ppm
f
Th/U ratio vs Age
Th / U ratio
Age in Ma
g
R3
R2
R1?
C2
number
Zircon Age (Ma)
C2 Age
Mean = 449.1 ± 2.6
MSWD = 2.5
inherited cores (C1)
n = 77
206Pb / 238U Age (Ma)
Mean = 282.6 ± 3.3
MSWD = 2.0
Mean = 315.4 ± 3.7
MSWD = 3.4
Mean = 414.1 ± 5.7
MSWD = 2.0

◂**Fig. 9** Zircon chronology: **a**–**c** Contrast charge images (CL) of representative zircon crystals from leucosomes LEU9. Scale is the same for all analysed zircons. Obtained $^{206}Pb/^{238}U$ ages are indicated next to spots. **d** Conventional Concordia diagram of two major age populations; inherited C1 cores are not shown. **e** Th–U concentration (ppm) in analysed zircons. **f** Th/U ratios versus age. **g** Probability density plot of $^{206}Pb/^{238}U$ ages with inserts showing the weighted mean ages for three rim populations (*R*1, *R*2, *R*3). Light grey bins mark ages that were rejected for weighted average calculations

sional shearing. This conclusion is supported by (i) S_R foliation that is concordant to the intrusive contact, (ii) bands of Streifengneis and aplitic dykes that are parallel to the contact, (iii) Schlingen folded apophyses and Schlingen that deformed older contact migmatites along the contact of the Streifengneis and the Val Nalps Gneiss, as well as (iv) a decrease in foliation spacing towards contact zones, expressed by a more evolved mylonitic foliation and a prominent grain size reduction (Figs. 2b and 5a). The corresponding most pronounced foliation (S_R) affects all major rock units and is deformed by the Schlingen phase (Fig. 10b).

(3) Schlingen phase. Field observations of the Tros outcrop show that the Schlingen phase must be considered as a polyphase event with multiple pulses of partial melting and compressional shearing. There is ample evidence to suggest that Schlingen formation is a combination of simultaneous shearing and folding of a pre-existing planar fabric (Fig. 10b). These older deformation events involving steepening are isoclinal small-scale folds (Ravetsch phase) as well as old foliations (S_T, S_R, S_r) being folded by the Schlingen phase. Also, multiple refolded banded amphibolites and Paradis Gneiss bands indicate fold interferences owing to multiple deformation events (Fig. 2b).

We conclude that the folding and associated shearing represent a continuum of deformation episodes rather than a single short-lived deformation event, based on the following:

(i) The Schlingen foliation shows different appearances ranging from a crenulation cleavage in the vicinity of the fold hinge to a penetrative axial plane foliation (Fig. 7d–f).

(ii) Whilst the map-scale Tros Schlinge plunges SW (252/70), second-order parasitic folds are more affected by fold interferences (D_V, D_A) and show considerable variations in plunge.

(iii) Axial plane parallel to -sub-parallel leucocratic dykes contain no foliation as opposed to older leucosomes (Le_A and Le_B in Fig. 7). This latter observation further suggests that, concomitant to the multiple deformation phases, simultaneous water-assisted partial melting occurred. Supporting evidence are the multiple foliations observed in the Tros outcrop and the evolution of leucosomes (S_{R1}, S_{R2}, S_S in Fig. 7d, e, f and Le_A, Le_B, Le_C in Fig. 7e). It is important to note that such a continuous polyphase deformation sequence, with potentially a locally rotating stress field, can yield leucosomes, which do not necessarily evolve strictly parallel to axial planes (Druguet 2019). We infer that the slight deviations of the leucosomes from the Tros axial plane can be interpreted in this sense.

(iv) At the kilometre scale, instead of a classical sequence of syn- and antiforms, the Schlingen in the Unteralptal rather consist of a succession of southwest closing folds, which laterally grade into high-strain shear zones being followed by the next southwest closing fold (Fig. 4a). The counterparts, namely northeast closing folds, are missing. The high-strain shear zones are a viable explanation for equally closing folds adjacent to each other (Fig. 4a). These syn-Schlingen high-strain shear zones cut pre-Variscan intrusive contacts between the Streifengneis, Val Nalps Gneiss and Paradis Gneiss. Some leucosomes are rotated and dragged into the shear zones (see also Pettke and Klaper 1992). Measured lineations of high-strain zones indicated a subvertical movement, which points to a transpressive setting during Variscan Schlingen folding. Hence, for the Schlingen phase, a strong strain partitioning within a general shear kinematic framework is typical with folds representing domains of horizontal compressional strain and the shear zones domains of highly localised shear strain with a reverse faulting component.

(v) Post-Schlingen deformation includes the Vermigel phase, the injection of the (meta)basic dykes, as well as the Alpine greenschist facies shearing (Table 1, Fig. 4b). The minor undulation of the Schlingen foliation is attributed to the Vermigel phase and is the first stage of post-Schlingen deformation (see Chapter 4.2.5). Whether the Vermigel phase post-dates the early Permian intrusions has yet to be established, since there is no outcrop exposing these relationships in the study area. The timing of the metabasic dykes is not yet entirely solved. Previous studies suggest that they indicate the latest intrusive event in the Gotthard nappe (Niggli 1944; Niggli and Niggli 1965; Oberhänsli 1986), which is also confirmed by observations in the Aar Massif (Schneeberger et al. 2016). Bussien et al. (2011) investigated metabasic dykes in the Teggiolo Zone, which yield an age of ~ 290 Ma. Our field observations indicate that metabasic dykes dissect the latest Schlingen-related leucocratic dykes (Le_C) and are not affected by Variscan high-strain shear zones.. Therefore, metabasic dykes are considered to be younger than the Schlingen folds. The orientation of metabasic dykes is steep and their lenticulargeometry is subparallel to

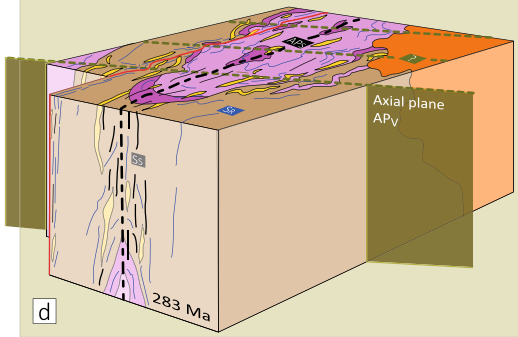

Vermigel Phase

- Locally open folds
- Weak foliation
- Minor deformation event

Lithologies

- Leucocratic dyke
- Granodiorite / Tonalite
- Streifengneis
- Metatexite
- Metasedimentary gneiss (GN)

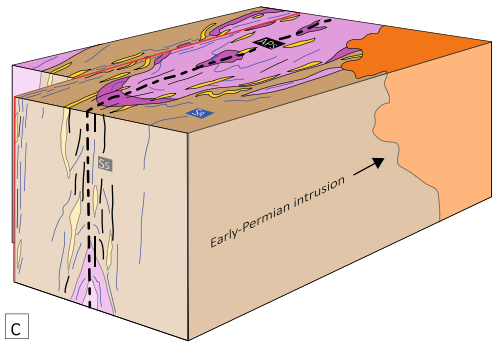

Early Permian Intrusions

Late to post-Variscan plutonic rocks

- Val Lavaz Group 299 - 295 Ma
- Pesciora Group 295 - 290 Ma

(e.g. Berger et al. 2017)

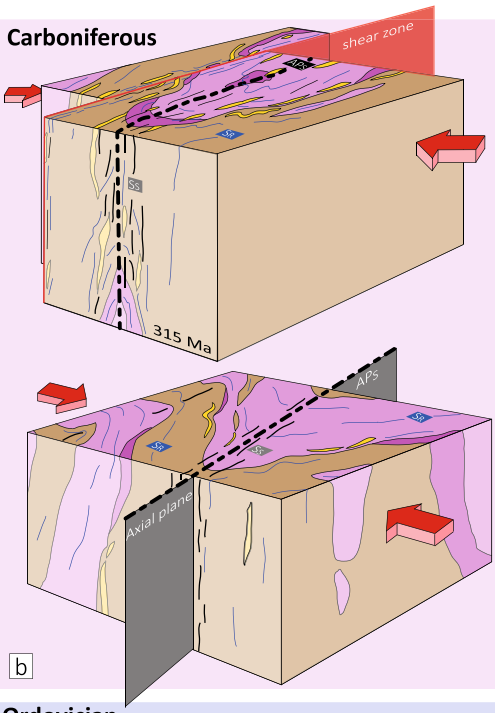

Schlingen Phase

Time Period	Stage	Tectonometamorphic events
315- 295 Ma	Mega shear zones *(e.g. Jacques et al. 2017, Ballèvre et al. 2018)*	Plate tectonic of crustal-scaled transpressive shear zones and oroclinal bending (EVSZ)
325- 315 Ma	Schlingen phase *(this study)*	Metamorphic peak with formation of syn-kinematic anatectical melts with increasing strain localisation (Proto EVSZ) **Schlingen tectonics** - Folding -> steep folds - Melting, migmatisation in fold hinge High-strain transpressive shear - zones
~ 340- 325 Ma	Proto-Schlingen phase *(e.g. Berger et al. 2017)*	**Early Schlingen formation** Lower crustal deformation Activation of steep anisotropies (foliation, bandings)

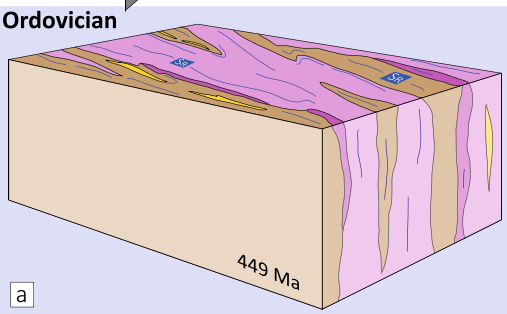

Intrusion of Streifengneis

- Pre-existing steep structures
- Synintrusive, metamorphic overprint
- Migmatisation in contact zones
- Ravetsch phase

◂**Fig. 10** Pre-Mesozoic evolution. **a** Ordovician to early-Silurian emplacement of the Streifengneis in steep metasedimentary sequences. **b** The Schlingen phase is considered as a continental-scaled tectonic event in relation to collision and transpression between Laurussia and Gondwana, affecting pre-existing subvertical anisotropies within peri-Gondwanan terranes. **c** Widespread early Permian intrusions (late Carboniferous intrusions after Mercolli et al. 1994) cut Schlingen structures and mark a younger time limit (Schaltegger 1994). **d** Vermigel phase is a temperature dependent deformation event with locally open folds and a weak foliation

the foliation planes of the Vermigel phase (Figs. 4b and 6d). This may suggest a synchronous injection with respect to Vermigel folding. The W-directed vergence of the open Vermigel folds suggest left-lateral shearing framework for this deformation stage (Fig. 4b). The brittle–ductile Alpine shear zones and their purely brittle reactivation clearly represent the youngest deformation, since they croscut all other structures mentioned above. Unravelling the exact timing of this Alpine deformation is, however, out of the scope of the present study and the interested reader is referred to (Marquer 1990; Oliot et al. 2014; Lützenkirchen and Löw 2011; Berger et al. 2017).

Tectonic evolution

In a plate-tectonic framework, the above discussed Schlingen tectonics are limited to the Southern Variscides, which were separated from the Moldanubian Zone, although both show a Gondwanan affinity. South of the Southern Variscides, foreland basins and undeformed Gondwana occurred (Fig. 11, e.g. Guillot and Ménot 2009). Due to the intense post-Variscan tectonics in Europe (mainly Permian-Jurassic extensional phases and Alpine convergence), the borders between undeformed Gondwana, Southern Variscides and Moldanubian Zone are only locally preserved. Owing to this uncertainty, we introduced a mixed zone in our reconstruction (Fig. 11). The main parts of the Southern Variscides are located today in the Alps, Maures Massif, Corsica and Sardinia (Fig. 11; e.g. Guillot and Ménot 2009; Simonetti et al. 2020a, b). Therefore, the former border between the Moldanubian Zone and the Southern Variscides is now located either inside the Alps or directly north of them underneath the Northalpine Foreland. It is intriguing to observe that the Schlingen structures are restricted to units of the Southern Variscan realm only. To understand this geodynamic point, the understanding for the spatially restricted formation of Schlingen needs to be discussed in terms of time. As already summarised in the introduction, the Variscan orogeny can be subdivided into an Eo-Variscan (400–380 Ma) event, a Meso-Variscan event (360–330 Ma) and a Neo-Variscan event (330–310 Ma), the latter having been transpression dominated (Putiš et al. 2009; Stampfli and Hochard 2009; von Raumer et al. 2013; Haas et al. 2020). Devonian and early Carboniferous crustal stacking, subduction and related arc magmatism of Ballèvre et al. (2018) are comparable to the Eo- and Meso-Variscan events. In addition, during late Carboniferous arcuate megastructures such as oroclines developed (Ibero-Amorican arc 315–297 Ma, Jacques et al. 2017). This Pennsylvanian event is contemporaneous to the evolution of the Schlingen. At the same time, magmatism occurred in the Moldanubian Zone as well as in the northern part of the Southern Variscides (Ballèvre et al. 2018, Figs. 10c and 12). The timing of Schlingen formation and transpressional deformation may be related to crustal scale shear zones, such as the East Variscan Shear Zone (EVSZ). Accepting a correlation of the EVSZ with the described structure inside the Gotthard nappe implies following questions: (1) What is the timing of the EVSZ activity? (2) What is the large-scale geometry of the EVSZ? and (3) What is the link between the EVSZ and the different Schlingen structures and oroclines (Fig. 11)? The main question will be the timing of the deformation. Simonetti et al. (2020a, b) propose a main activity between 330 and 320 Ma (their Fig. 7). Elter et al. (2020) connect the EVSZ with different sedimentary basins related to strike-slip deformation in the Alps, Corsica and Sardegna (Stephanian and younger in age). Accepting a long-term activity of the EVSZ (~ 30 Ma), all these interpretations overlap (Padovano et al. 2012; Ballèvre et al. 2018; Simonetti et al. 2018, 2020a, b; Elter et al. 2020). However, the plate tectonic interpretation would differ and different scales have to be considered. In contrast to a crustal scale shear zone as a major strike-slip zone, an alternative concept of different branches implies a large-scale corridor of deformation (Fig. 11). Examples of such a corridor are shear zones with (sub-)vertical mylonitic foliation bands of several hundred metres width (Ballèvre et al. 2014; Advokaat et al. 2014; Simonetti et al. 2020b). Some of these transpressive shear zones were active simultaneously with the formation of large-scale folds (Simonetti et al. 2020b). The correlation of the EVSZ as a large-scale deformation corridor with different strike-slip branches and Schlingen indicates transpressive deformation.

This is in contrast to the general basin evolution, which requires a transtentional setting in the same time interval (Elter et al. 2020). A contemporaneous local transpressional and transtensional deformation (= releasing and restraining bends) would integrate the different detailed observations.

The proposed structural model requires shearing and folding, which is consistent with the Carboniferous collisional tectonics (Fig. 11a). Moreover, these structures are contemporaneous to our newly dated Schlingen phase. In contrast, the distribution of magmatism indicates larger-scale lateral movements. In the Aiguilles Rouge Massif, the Schlingen

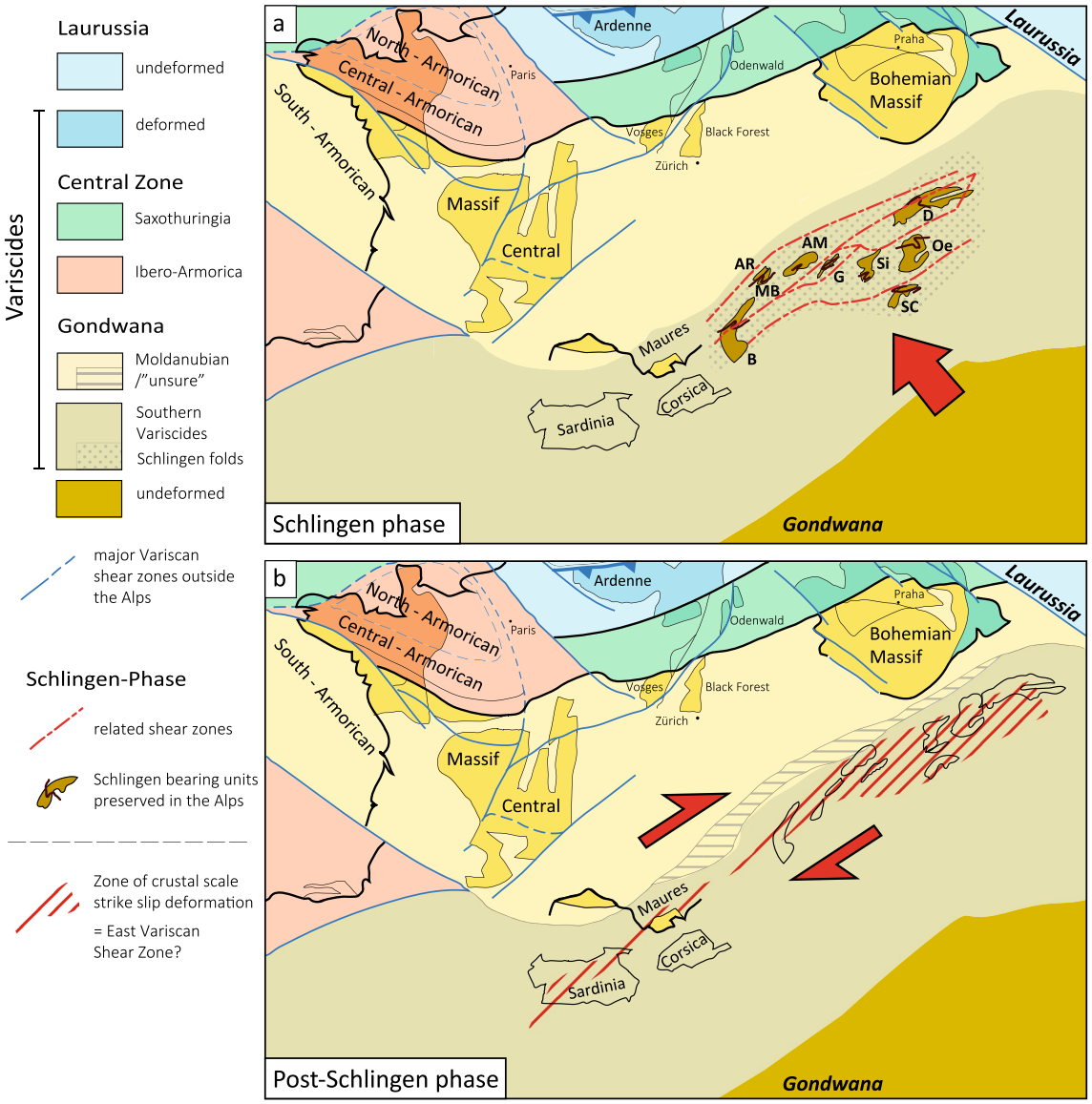

Fig. 11 Situations of the Neo-Variscides. **a** Sketch of a possible reconstruction of the Southern Variscides during the late Carboniferous Schlingen phase (see text for definition). Note the necessary transpressional deformation to reorganise the units within the Alpine realm (*A* Argentera Massif, *B* Belledonne Massif, *MB* Mont Blanc Massif, *AR* Aguilles Rouges Massif, *AM* Aar Massif, *G* Gotthard nappe, *Oe* Oetztal nappe, *Si* Silvretta nappe, *D* Defereggen Alps, *SC* Strona-Ceneri zone). For details of the Variscides outside the box, see Ballèvre et al. 2018. **b** The situation after the transpressional stage of (**a**) indicates a strike-slip situation or a more transtensional stage, which is well known from the Permian. Both figures are generally redrawn after Ballèvre et al. 2018 with modifications regarding the Alpine realm

phase is terminated by extensive sheet-like intrusions of peraluminous granitic melts (e.g. ~ 307 Ma, Bussy et al. 2000). In comparison with the neighbouring Mont Blanc and Aar Massif, the Gotthard nappe lacks Carboniferous magmatism, which is also the case for the Austroalpine and Southalpine basement units (Fig. 12). Therefore, we tentatively propose for the Gotthard nappe a Carboniferous position further to the east (Fig. 11a). This paleo-location has several implications: (i) given the overall dextral shear, the Gotthard nappe, as well as the Austroalpine and Southalpine basement units were displaced westwards during late Carboniferous/Permian times; (ii) the emplacement of the Gotthard nappe close to the Aar Massif occurred during strike-slip movements. These two data sets (inferred collision and strike-slip movements) can be seen as a single long-lived (active over 30 Ma) or as a two-stage process (a Carboniferous transpressional phase, followed by a local Permian transtensional phase; e.g. compare timing in Simonetti et al. 2020a, b; Stephan et al. 2019; Pohl et al. 2018). Our data indicate that late Carboniferous Schlingen tectonics, related to oblique collision

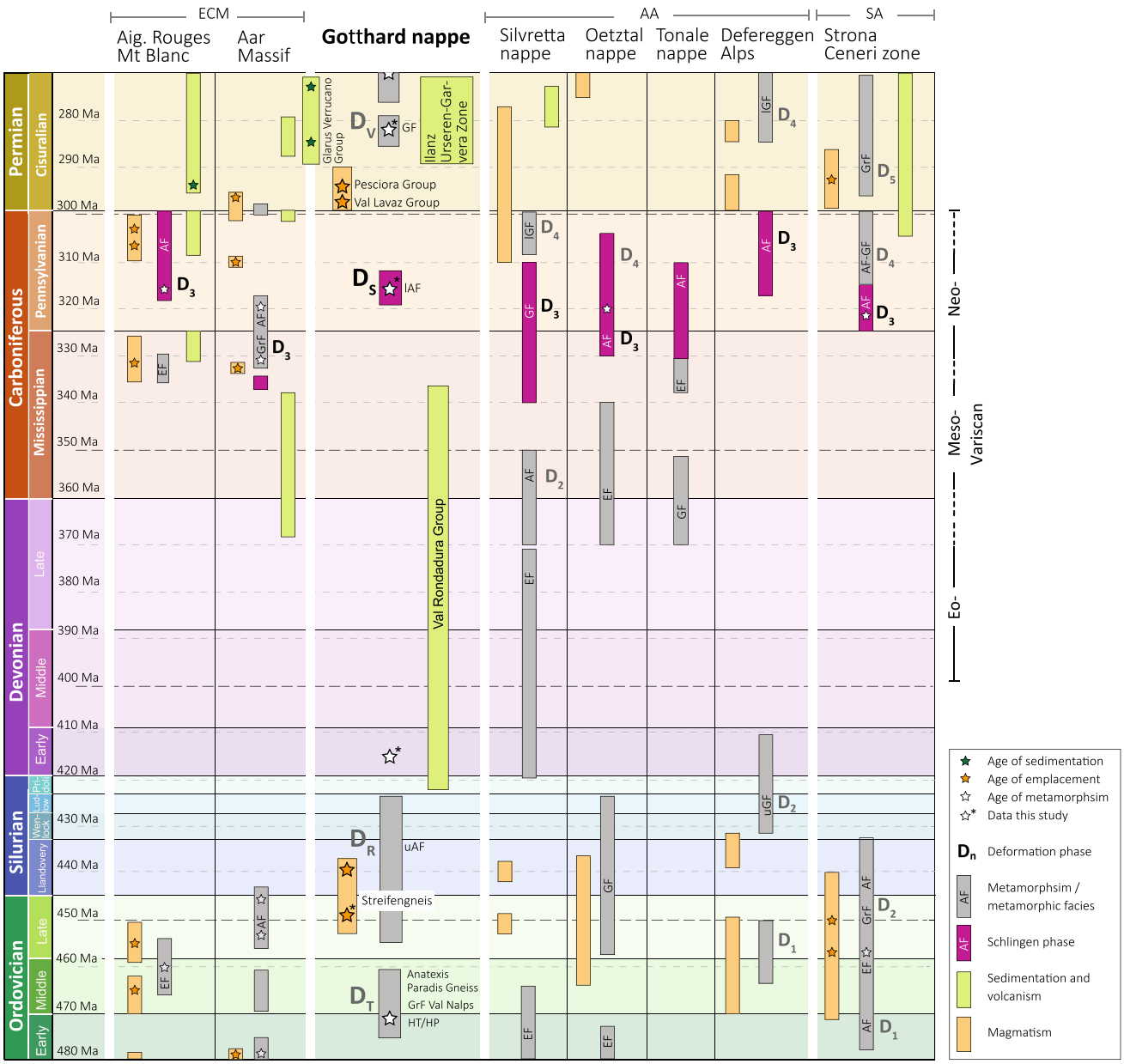

Fig. 12 Orogenic timetable for pre-Mesozoic evolution of Schlingen containing basements in the Alpine belt. The Schlingen phase (D_S or D_3) spans over 40 Ma from 340 to 300. Metamorphic facies: *l,u* prefixes indicating lower and upper; *GF* greenschist facies, *AF* amphibolite facies, *GrF* granulite facies, *EF* eclogite facies. Column of Aar Massif is modified after Berger et al. 2017. Full list of references is provided in appendix A

(~transpressional at local scale; see also Guillot and Ménot 2009), includes large-scale strain partitioning. Furthermore, the model proposes that the pre-existing steep anisotropies coalesced by progressive non-coaxial transpression into a branched network of localised high-strain shear zones. In between such high-strain shear zones, regional compression prevailed and induced continuous formation of Schlingen structures (Fig. 11a). Despite the general simultaneity of anastomosing shear zones around compressed lenses with internal Schlingen folding, we propose dominance of a pure shear component during this collisional stage. This is followed or continued into more strike-slip dominated deformation to explain the difference in magmatism (Fig. 11b; see above).

Summary

The investigated kilometre-scale Schlingen fold in the Gotthard nappe is an amphibolite facies regional structure with a steep fold axis and axial plane. The eponymous Schlingen phase expresses a polyphase deformation, which is associated with Variscan crustal-scale shear zones that affected units of the Southern Variscides within peri-Gondwana terranes. For the Central Alps we draw the following conclusions:

(i) The northern rim of Gondwana became steeply structured during the Ordovician time. Consequently, characteristic subvertical pre-Schlingen anisotropies formed, such as foliations and bandings.
(ii) During oblique collision between Laurussia and Gondwana, a strong strain partitioning formed crustal-scale Schlingen folds (315 ± 4 Ma) and strike-slip zones. After Schlingen folding, the strike-slip zones coalesced and plate motions triggered the formation of the EVSZ in its eastern part.
(iii) Schlingen in the Gotthard nappe developed under amphibolite-facies conditions and concurrent water-fluxed partial melting migmatised Ordovician granitoids (Streifengneis 449 ± 3 Ma) and older migmatites (Paradis Gneiss). Melt segregation during the Schlingen phase was variable, but commonly occurred in fold hinges, fold limbs and along shear zones of Schlingen structures.
(iv) Variscan post-Schlingen deformation (Vermigel phase) locally produced open folds (D_V) and penetrative foliation at similar metamorphic conditions as the Schlingen phase documenting ongoing transpression.

Supplementary Information The online version contains supplementary material available at https://doi.org/10.1007/s00531-022-02247-5.

Acknowledgements Many thanks go to Francesca Piccoli and Alice Vho for their help and contribution in sample processing and isotope dating. Furthermore, Mario Bühler would like to thank Renata da Silva Schmitt, Liliane and Urs Friedli and Lukas Neubacher for assistance in the field. The shepherds Rolf and Michael Wiesiolek with Katharina and Lorenz are acknowledged for hosting Mario Bühler during extensive field work in summer 2019. We thank P.Manzotti, Niko Froitzheim and an anonymous reviewer for their helpful comments on an earlier version of the manuscript.

Author contributions RZ, AB and MH designed the study. MB performed the mapping, description, structural analysis, isotope dating and isotope data compilation. DR supervised the isotope dating and ran the analytics. All authors contributed to writing the article.

Funding Open access funding provided by University of Bern.

Availability of data and material All used data are available in the manuscript and the supplementary data.

Declarations

Conflict of interest The authors declare no competing interests.

Ethics approval and consent to participate Not applicable.

Consent for publication Not applicable.

References

Abrecht J (1994) Geologic units of the Aar massif and their pre-Alpine rock associations: a critical review. Schweiz Min Petr Mitt 74:5–27

Abrecht J, Biino GG, Mercolli I (1991) Mafic-ultramafic rock associations in the Aar, Gotthard and Tavetsch massifs of the Helvetic domain in the Central Swiss Alps: markers of ophiolitic pre-Variscan sutures, reworked by polymetamorphic events? Schweiz Min Petr Mitt 71:295–300

Advokaat EL, Van Hinsbergen DJJ, Kaymakci N et al (2014) Late cretaceous extension and Palaeogene rotation-related contraction in Central Anatolia recorded in the Ayhansla basin. Int Geol Rev 56:1813–1836. https://doi.org/10.1080/00206814.2014.954279

Ambühl E (1929) Petrographie und Geologie des zentralen Gotthardmassivs südlich Andermatt. A.-G. Gebr. Leemann & Co., Zürich

Andreatta C (1948) La Linea di Peio nel massiccip dell'Ortler e le sue miloniti. Acta Geol Alp 1:1–63

Arnold A (1970) On the history of the Gotthard Massif (Central Alps, Switzerland). Eclogae Geol Helv 63:29–30

Arnold A (1972) Zur Entstehung der Kalksilikatfels-Einschlüsse in den gotthardmassivischen Gneisen (Eine Ergänzung). Schweizerische Mineral Und Petrogr Mitteilungen 52:553–555

Bächlin R (1937) Geologie und Petrographie des M. Tamaro-Gebietes (südliches Tessin). Schweiz Min Petr Mitt 17:1–79

Ballèvre M, Catalán JR, López-Carmona A et al (2014) Correlation of the nappe stack in the Ibero-Armorican arc across the Bay of Biscay: a joint French-Spanish project. Geol Soc London Spec Publ 405:77–113. https://doi.org/10.1144/SP405.13

Ballèvre M, Manzotti P, Dal Piaz GV (2018) Pre-Alpine (Variscan) inheritance: a key for the location of the future Valaisan basin (Western Alps). Tectonics 37:786–817. https://doi.org/10.1002/2017TC004633

Berger A, Schmid SM, Engi M et al (2011) Mechanisms of mass and heat transport during Barrovian metamorphism: a discussion based on field evidence from the Central Alps (Switzerland/Northern Italy). Tectonics. https://doi.org/10.1029/2009TC002622

Berger A, Mercolli I, Herwegh M, et al (2017) Geological map of the Aar Massif, Tavetsch and Gotthard nappes: Swiss Geological Survey, Wabern

Biino J, Mercolli GG (1991) Mafic-ultramafic rock associations in the Aar, Gotthard and Tavetsch massifs of the Helvetic domain in the Central Swiss Alps: markers of ophiolitic pre-Variscan sutures, reworked by polymetamorphic events? Schweiz Min Petr Mitt 71:295–300

Black LP, Kamo SL, Allen CM et al (2003) TEMORA 1: a new zircon standard for Phanerozoic U-Pb geochronology. Chem Geol 200:155–170. https://doi.org/10.1016/S0009-2541(03)00165-7

Bonin B, Brändlein P, Bussy F et al (1993) Late Variscan magmatic evolution of the alpine basement. Pre-Mesozoic geology in the Alps. Springer, Berlin Heidelberg, pp 171–201

Boriani A, Origoni EG, Borghi A, Caironi V (1990) The evolution of the "Serie dei Laghi" (Strona-Ceneri and Scisti dei Laghi): the upper component of the Ivrea-Verbano crustal section; Southern Alps, North Italy and Ticino, Switzerland. Tectonophysics 182:103–118. https://doi.org/10.1016/0040-1951(90)90345-9

Bussien D, Bussy F, Magna T, Masson H (2011) Timing of Palaeozoic magmatism in the Maggia and Sambuco nappes and paleogeographic implications (Central Lepontine Alps). Swiss J Geosci 104:1–29. https://doi.org/10.1007/s00015-010-0049-6

Bussy F, Hernandez J, Von Raumer J (2000) Bimodal magmatism as a consequence of the post-collisional readjustment of the thickened Variscan continental lithosphere (Aiguilles Rouges-Mont Blanc Massifs, Western Alps). Spec Pap Geol Soc Am 350:221–233. https://doi.org/10.1130/0-8137-2350-7.221

Campani M, Mancktelow N, Seward D et al (2010) Geochronological evidence for continuous exhumation through the ductile-brittle transition along a crustal-scale low-angle normal fault: Simplon fault zone, central Alps. Tectonics. https://doi.org/10.1029/2009TC002582

Carosi R, Montomoli C, Tiepolo M, Frassi C (2012) Geochronological constraints on post-collisional shear zones in the Variscides of Sardinia (Italy). Terra Nova 24:42–51. https://doi.org/10.1111/j.1365-3121.2011.01035.x

Corfu F, Hanchar JM, Hoskin PWO, Kinny P (2003) Atlas of zircon textures. Rev Mineral Geochemistry 53:469–500. https://doi.org/10.2113/0530469

Del Moro A, Martin S, Prosser G (1999) Migmatites of the Ulten zone (NE Italy), a record of melt transfer in deep crust. J Petrol 40:1803–1826. https://doi.org/10.1093/petroj/40.12.1803

Druguet E (2019) Deciphering the presence of axial-planar veins in tectonites. Geosci Front 10:2101–2115. https://doi.org/10.1016/j.gsf.2019.02.005

Edel JB, Schulmann K, Lexa O, Lardeaux JM (2018) Late Palaeozoic palaeomagnetic and tectonic constraints for amalgamation of Pangea supercontinent in the European Variscan belt. Earth-Science Rev 177:589–612. https://doi.org/10.1016/j.earscirev.2017.12.007

Etter U, Low S, Wyss R (1999) Die Strukturgeologie des Gebietes Lukmanierpass - Piora - Leventina. Geologie Alptransit: Vorerkundung und Prognose der Basistunnels am Gotthard und am Lötschberg. A A Balkema, US, pp 109–116

Elter FM, Gaggero L, Mantovani F et al (2020) The Atlas-East Variscan -Elbe shear system and its role in the formation of the pull-apart Late Palaeozoic basins. Int. J. Earth Sci. 109:739–760. https://doi.org/10.1007/s00531-020-01830-y

Faure M, Li XH, Lin W (2017) The northwest-directed "Bretonian phase" in the French Variscan belt (Massif Central and Massif Armoricain): a consequence of the early carboniferous Gondwana-Laurussia collision. Comptes Rendus - Geosci 349:126–136. https://doi.org/10.1016/j.crte.2017.05.002

Förster H (1967) Kristallisation und Tektonik des Schneeberger Gesteinszuges. Geol Rundschau 56:480–494. https://doi.org/10.1007/BF01848738

Fréville K, Trap P, Faure M et al (2018) Structural, metamorphic and geochronological insights on the Variscan evolution of the Alpine basement in the Belledonne Massif (France). Tectonophysics 726:14–42. https://doi.org/10.1016/j.tecto.2018.01.017

Frey M, Desmons J, Neubauer F (1999) The new metamorphic map of the Alps, 1: 500 000. Schweiz Min Petr Mitt 79:1–4. https://doi.org/10.5169/seals-60194

Gardien V, Lardeaux J-M, Ledru P et al (1997) Metamorphism during late orogenic extension: insights from the French Variscan belt. Bull La Soc Geol Fr 168:271–286

Guillot S, Ménot RP (2009) Paleozoic evolution of the external crystalline Massifs of the Western Alps. Comptes Rendus - Geosci 341:253–265. https://doi.org/10.1016/j.crte.2008.11.010

Guillot S, Di Paola S, Ménot RP et al (2009) Suture zones and importance of strike-slip faulting for Variscan geodynamic reconstructions of the external crystalline Massifs of the western Alps. Bull La Soc Geol Fr 180:483–500. https://doi.org/10.2113/gssgfbull.180.6.483

Haas I, Eichinger S, Haller D et al (2020) Gondwana fragments in the eastern Alps: a travel story from U/Pb zircon data. Gondwana Res 77:204–222. https://doi.org/10.1016/j.gr.2019.07.015

Herwegh M, Berger A, Baumberger R et al (2017) Large-scale crustal-block-extrusion during late Alpine collision. Sci Rep 7:1–10. https://doi.org/10.1038/s41598-017-00440-0

Herwegh M, Berger A, Glotzbach C et al (2020) Late stages of continent-continent collision: timing, kinematic evolution, and exhumation of the northern rim (Aar Massif) of the Alps. Earth-Sci Rev. https://doi.org/10.1016/j.earscirev.2019.102959

Horstwood MSA, Foster GL, Parrish RR et al (2003) Common-Pb corrected in situ U-Pb accessory mineral geochronology by LA-MC-ICP-MS. J Anal at Spectrom 18:837–846. https://doi.org/10.1039/b304365g

Hoskin PWO, Schaltegger U (2003) The composition of zircon and igneous and metamorphic petrogenesis. Rev Miner Geochem 53:27–62. https://doi.org/10.2113/0530027

Huber HM (1943) Physiographie und Genesis der Gesteine im südöstlichen Gotthardmassiv. Schweiz Min Petr Mitt 23:72–260

Jacob J, Guillot S, Rubatto D et al (2021) Carboniferous high- P metamorphism and deformation in the Belledonne Massif (Western Alps). J Metamorph Geol 39:1009–1044. https://doi.org/10.1111/jmg.12600

Jacques D, Vieira R, Muchez P, Sintubin M (2017) Transpressional folding and associated cross-fold jointing controlling the geometry of post-orogenic vein-type W-Sn mineralization: examples from Minas da Panasqueira, Portugal. Miner Depos 53:171–194. https://doi.org/10.1007/s00126-017-0728-6

Jouffray F, Spalla MI, Lardeaux JM et al (2020) Variscan eclogites from the Argentera-Mercantour Massif (external crystalline Massifs, SW Alps): a dismembered cryptic suture zone. Int J Earth Sci 109:1273–1294. https://doi.org/10.1007/s00531-020-01848-2

Klaper EM (1982) Deformation und metamorphose in der nördlichen Maggia-zone. Schweiz Min Petr Mitt 62:47–76

Klaper EM (1985) Deformation history and metamorphic mineral growth along the Pennine frontal thrust (Wallis, Ticino), Switzerland. PhD Thesis, ETH Zürich. https://doi.org/10.3929/ETHZ-A-000343127

Kroner U, Romer RL (2013) Two plates - many subduction zones: the Variscan orogeny reconsidered. Gondwana Res 24:298–329. https://doi.org/10.1016/j.gr.2013.03.001

Kroner U, Mansy JL, Mazur S et al (2008) Variscan tectonics. Cent Eur 1:599–664. https://doi.org/10.1144/cev1p.11

Labhart T (2005) Blatt 1251 Val Bedretto. Geol. Atlas Schweiz 1:25 000, Erläut 68.
Labhart T, Renner F (2012) Blatt 1231 Urseren. Geol Atlas der Schweiz 1:25 000, Erläut 133.
Laurent V, Huet B, Labrousse L et al (2017) Extraneous argon in high-pressure metamorphic rocks: distribution, origin and transport in the Cycladic Blueschist Unit (Greece). Lithos 272–273:315–335. https://doi.org/10.1016/j.lithos.2016.12.013
Lopez-Sanchez MA, Aleinikoff JN, Marcos A et al (2016) An example of low-Th/U zircon overgrowths of magmatic origin in a late orogenic variscan intrusion: the San Ciprián massif (NW Spain). J Geol Soc London 173:282–291. https://doi.org/10.1144/jgs2015-071
Ludwig KR (2012) Isoplot 3.75: a geochronological toolkit for Microsoft Excel. Berkeley CA Berkeley Geochronol Cent Spec Publ 5:1–75
Lützenkirchen VH (2002) Structural geology and hydrogeology of brittle fault zones in the central and eastern Gotthard massif, Switzerland. PhD Thesis, ETH Zürich. https://doi.org/10.3929/ETHZ-A-004522949
Lützenkirchen V, Löw S (2011) Late Alpine brittle faulting in the Rotondo granite (Switzerland): deformation mechanisms and fault evolution. Swiss J Geosci 104:31–54. https://doi.org/10.1007/s00015-010-0050-0
Malavieille J, Guihot P, Costa S et al (1990) Collapse of the thickened Variscan crust in the French Massif Central: Mont Pilat extensional shear zone and St. Etienne Late Carboniferous basin. Tectonophysics 177:139–149. https://doi.org/10.1016/0040-1951(90)90278-G
Manzotti P, Rubatto D, Darling J et al (2012) From Permo-Triassic lithospheric thinning to Jurassic rifting at the Adriatic margin: petrological and geochronological record in Valtournenche (Western Italian Alps). Lithos 146–147:276–292. https://doi.org/10.1016/j.lithos.2012.05.007
Martin S, Gaston G, Prosser G et al (1998) Evolution of the deep crust at the junction Austroalpine/Southalpine: the Tonale Nappe. Mem Di Sci Geol 50:3–50
Martínez Catalan JR, Arenas R, Díagarcía F et al (2007) Space and time in the tectonic evolution of the north western Iberian Massif: implications for the Variscan belt. Memoir of the geological society of America. Geological Society of America, US, pp 403–423. https://doi.org/10.1130/2007.1200(21)
Marquer D (1990) Structures et déformation alpine dans les granités hercyniens du massif du Gothard (Alpes centrales suisses). Eclogae Geol Helv 83:77–97
Mercolli I, Biino GG, Abrecht J (1994) The lithostratigraphy of the pre-Mesozoic basement of the Gotthard Massif: a review. Schweiz Min Petr Mitt 74:29–40
Milnes AG (1974) Structure of the Pennine zone (Central Alps): a new working hypothesis. Bull Geol Soc Am 85:1727–1732. https://doi.org/10.1130/0016-760
Niggli E (1944) Das westliche Tavetscher Zwischenmassiv und der angrenzende Nordrand des Gotthardmassivs. Schweiz Min Petr Mitt 24:58–301
Niggli E, Niggli CB (1965) Karten der verbreitung einiger mineralien der alpidischen metamorphose in den Schweizer Alpen (stilpnomelan, alkali-amphibol, chloritoid, staurolith, disthen, sillimanit). Eclogae Geol Helv 58:335–368
Oberhänsli R (1986) Geochemistry of meta-lamprophyres from the Central Swiss Alps. Schweiz Min Petr Mitt 66:315–342
Oliot E, Goncalves P, Schulmann K et al (2014) Mid-crustal shear zone formation in granitic rocks: constraints from quantitative textural and crystallographic preferred orientations analyses. Tectonophysics 612–613:63–80. https://doi.org/10.1016/j.tecto.2013.11.032
Padovano M, Elter FM, Pandeli E, Franceschelli M (2012) The east Variscan shear zone: new insights into its role in the late carboniferous collision in southern Europe. Int Geol Rev 54:957–970
Paton C, Hellstrom J, Paul B et al (2011) Iolite: freeware for the visualization and processing of mass spectrometric data. J Anal at Spectrom 26:2508–2518. https://doi.org/10.1039/c1ja10172b
Petrus JA, Kamber BS (2012) VizualAge: a novel approach to laser ablation ICP-MS U-Pb geochronology data reduction. Geostand Geoanalytical Res 36:247–270. https://doi.org/10.1111/j.1751-908X.2012.00158.x
Pettke T, Klaper EM (1992) Zur petrographie und deformationsgeschichte des südöstlichen Gotthardmassivs (petrology and deformation of the southeastern Gotthard massif). Schweiz Min Petr Mitt 72:197–212
Pfiffner OA (2006) Thick-skinned and thin-skinned styles of continental contraction. Spec Pap Geol Soc Am. https://doi.org/10.1130/2006.2414(09)
Pfiffner O (2014) Geology of the Alps. Wiley-Blackwell, London
Pohl F, Froitzheim N, Obermüller G et al (2018) Kinematics and age of syn-intrusive detachment faulting in the Southern Alps: evidence for early Permian crustal extension and implications for the Pangea A versus B controversy. Tectonics 37:3668–3689. https://doi.org/10.1029/2018TC004974
Putiš M, Ivan P, Kohut M et al (2009) Meta-igneous rocks of the West-Carpathians basement as an indicator of early Paleozoic extension-rifting/breakup events. Bull La Soc Geol Fr 180:461–471. https://doi.org/10.2113/gssgfbull.180.6.461
Rast M, Galli A, Ruh JB et al (2022) Geology along the Bedretto tunnel: kinematic and geochronological constraints on the evolution of the Gotthard Massif (Central Alps). Swiss J Geosci 115:8. https://doi.org/10.1186/s00015-022-00409-w
Ricchi E, Bergemann CA, Gnos E et al (2019) Constraining deformation phases in the Aar Massif and the Gotthard Nappe (Switzerland) using Th-Pb crystallization ages of fissure monazite-(Ce). Lithos 342–343:223–238. https://doi.org/10.1016/j.lithos.2019.04.014
Rubatto D (2017) Zircon: the metamorphic mineral. Rev Miner Geochem 83:261–296. https://doi.org/10.2138/rmg.2017.83.9
Rubatto D, Hermann J, Berger A, Engi M (2009) Protracted fluid-induced melting during Barrovian metamorphism in the Central Alps. Contrib Miner Pet 158:703–722. https://doi.org/10.1007/s00410-009-0406-5
Rubatto D, Chakraborty S, Dasgupta S (2013) Timescales of crustal melting in the higher Himalayan crystallines (Sikkim, Eastern Himalaya) inferred from trace element-constrained monazite and zircon chronology. Contrib Miner Pet 165:349–372. https://doi.org/10.1007/s00410-012-0812-y
Rutter E, Brodie K, James T, Burlini L (2007) Large-scale folding in the upper part of the Ivrea-Verbano zone, NW Italy. J Struct Geol 29:1–17. https://doi.org/10.1016/j.jsg.2006.08.01310.2138/rmg.2017.83.9
Sander B (1914) Bemerkungen uber tecktonische Gesteinfazies und Tecktonik des Grundgebirges. Verhandlungen geologische Reichsanstalt. Geological Federal Institute Vienna, Vienna, pp 220–240
Sassi F, Cavazzini G, Visonà D, Moro A (1985) Radiometric geochronology in the eastern Alps: results and problems (Italy). Rend Della Soc Ital Di Miner e Pet 40:187–224
Schaltegger U (1984) Geologie und Petrographie der Gneiszone von Erstfeld in der Umgebung des Sustenpasses, Aarmassiv (unpublished). Diploma thesis, University of Bern
Schaltegger U (1994) Unravelling the pre-Mesozoic history of Aar and Gotthard massifs (Central Alps) by isotopic dating - a review. Schweiz Min Petr Mitt 74:41–51

Schaltegger U (2000) U-Pb geochronology of the southern black forest Batholith (Central Variscan Belt): timing of exhumation and granite emplacement. Int J Earth Sci 88:814–828. https://doi.org/10.1007/s005310050308

Schaltegger U, Corfu F (1995) Magmatisme et tectonique tardi-varisque de type "basin and range" dans les Alpes Centrales: évidence geochronologique U-Pb. Geodin Acta 8:82–98. https://doi.org/10.1080/09853111.1995.11105276

Schmidegg O (1936) Steilachsige Tektonik und Schlingenbau auf der Südseite der Tiroler Zentralalpen. Jb Geol B-A 86:115–149

Schmidt K (1964) Zum Bau der südlichen Ötztaler und Stubaier Alpen. Zeitschrift Der Dtsch Geol Gesellschaft 116:455–469

Schmidt K (1965) Zum Schlingenbau Tiefer Gebirgsetagen. Krystalinkium 3:133–156

Schneeberger R, Berger A, Herwegh M et al (2016) GTS phase VI - LASMO: Geology and structures of the GTS and Grimsel region. Nagra Arbeitsbericht NAB 16:27

Schulz B (1988) Deformation, metamorphose und petrographie im ostalpinen Altkristallin südlich des Tauernfensters (südliche Deferegger Alpen, Österreich). Schweiz Min Petr Mitt 68:295–300. https://doi.org/10.5169/seals-52077

Schulz B, von Raumer JF (2011) Discovery of Ordovician-Silurian metamorphic monazite in garnet metapelites of the Alpine external Aiguilles Rouges Massif. Swiss J Geosci 104:67–79. https://doi.org/10.1007/s00015-010-0048-7

Schulz B, Steenken A, Siegesmund S (2008) Geodynamic evolution of an Alpine terrane-the Austroalpine basement to the south of the Tauern Window as a part of the Adriatic Plate (eastern Alps). Geol Soc Spec Publ 298:5–44. https://doi.org/10.1144/SP298.2

Schuster R, Stüwe K (2008) Permian metamorphic event in the Alps. Geology 36:603–606. https://doi.org/10.1130/G24703A.1

Sergeev SA, Steiger RH (1993) High-percision U-Pb single zircon dating of Variscan and Caledonian magmatic cycles in the Gotthard massif, Central Swiss Alps. Terra Abstr 5:394–395

Sergeev SA, Meier M, Steiger RH (1995) Improving the resolution of single-grain U/Pb dating by use of zircon extracted from feldspar: application to the Variscan magmatic cycle in the central Alps. Earth Planet Sci Lett 134:37–51. https://doi.org/10.1016/0012-821X(95)00105-L

Simonetti M, Carosi R, Montomoli C et al (2018) Kinematic and geochronological constraints on shear deformation in the Ferriere-Mollières shear zone (Argentera-Mercantour Massif, Western Alps): implications for the evolution of the Southern European Variscan Belt. Int J Earth Sci 107:2163–2189. https://doi.org/10.1007/s00531-018-1593-y

Simonetti M, Carosi R, Montomoli C et al (2020a) Transpressive deformation in the Southern European Variscan Belt: new insights from the Aiguilles Rouges Massif (Western Alps). Tectonics 39:1–24. https://doi.org/10.1029/2020TC006153

Simonetti M, Carosi R, Montomoli C et al (2020b) Timing and kinematics of flow in a transpressive dextral shear zone, Maures Massif (Southern France). Int J Earth Sci. https://doi.org/10.1007/s00531-020-01898-6

Sláma J, Košler J, Condon DJ et al (2008) Plešovice zircon - A new natural reference material for U-Pb and Hf isotopic microanalysis. Chem Geol 249:1–35. https://doi.org/10.1016/j.chemgeo.2007.11.005

Sölva H, Thöni M, Grasemann B, Linner M (2001) Emplacement of eo-Alpine high-pressure rocks in the Austroalpine Ötztal complex (Texel group, Italy/Austria). Geodin Acta 14:345–360. https://doi.org/10.1016/S0985-3111(01)01072-5

Sölva H, Grasemann B, Thöni M et al (2005) The Schneeberg normal fault zone: normal faulting associated with cretaceous SE-directed extrusion in the Eastern Alps (Italy/Austria). Tectonophysics 401:143–166. https://doi.org/10.1016/j.tecto.2005.02.005

Spiess R, Cesare B, Mazzoli C et al (2010) The crystalline basement of the Adria microplate in the eastern Alps: a review of the palaeostructural evolution from the Neoproterozoic to the Cenozoic. Rend Lincei 21:31–50. https://doi.org/10.1007/s12210-010-0100-6

Spitz A, Dyhrenfurth G (1914) Monographie der engadiner dolomiten zwischen schuls, scanfs und dem stilfserjoch. Kommission bei A. Francke, Bern

Stampfli G, Borel GD (2002) A plate tectonic model for the Paleozoic and Mesozoic constrained by dynamic plate boundaries and restored synthetic oceanic isochrons. Earth Planet Sci Lett 196:17–33. https://doi.org/10.1016/S0012-821X(01)00588-X

Stampfli GM, Hochard C (2009) Plate tectonics of the Alpine realm. Geol Soc Spec Publ 327:89–111. https://doi.org/10.1144/SP327.6

Steck A, Della Torre F, Keller F et al (2013) Tectonics of the Lepontine Alps: ductile thrusting and folding in the deepest tectonic levels of the Central Alps. Swiss J Geosci 106:427–450. https://doi.org/10.1007/s00015-013-0135-7

Stephan T, Kroner U, Romer RL, Rösel D (2019) From a bipartite Gondwanan shelf to an arcuate Variscan belt: the early Paleozoic evolution of northern Peri-Gondwana. Earth-Science Rev 192:491–512. https://doi.org/10.1016/j.earscirev.2019.03.012

Thöni M (1999) A review of geochronological data from the Eastern Alps. Swiss J Geosci Suppl 79:209–230

Van Gool JAM, Kemme MMJ, Schreurs GMMF (1987) Structural investigations along an E-W cross-section in the southern Ötztal Alps. In: Flügel HW, Faupl P (eds) Geodynamics of the eastern Alps. Deuticke, Wien, pp 214–225

Von Raumer JF, Bussy F (2004) Mont Blanc and Aiguilles Rouges Geology of their polymetamorphic Basement (External Massifs, Western Alps, France-Switzerland). In: Mémoires de Géologie. Lausanne

Von Raumer JF, Neubauer F (1993) History of geological investigations in the Pre-Triassic basement of the Alps. Pre-Mesozoic geology in the Alps. Springer, Berlin Heidelberg, pp 55–63

Von Raumer JF, Bussy F, Schaltegger U et al (2013) Pre-mesozoic alpine basements-their place in the European paleozoic framework. Bull Geol Soc Am 125:89–108. https://doi.org/10.1130/B30654.1

Watt GR, Griffin BJ, Kinny PD (2000) Charge contrast imaging of geological materials in the environmental scanning electron microscope. Am Mineral 85:1784–1794. https://doi.org/10.2138/am-2000-11-1221

Wehrens P, Baumberger R, Berger A, Herwegh M (2017) How is strain localized in a meta-granitoid, mid-crustal basement section? Spatial distribution of deformation in the central Aar massif (Switzerland). J Struct Geol 94:47–67. https://doi.org/10.1016/j.jsg.2016.11.004

Wenk E (1934) Beiträge zur petrographie und geologie des Silvrettakristallins Graubünden. A.-G. Gebr. Leemann & Co., Zürich

Wiedenbeck M, Hanchar JM, Peck WH et al (2004) Further characterisation of the 91500 zircon crystal. Geostand Geoanalytical Res 28:9–39. https://doi.org/10.1111/j.1751-908X.2004.tb01041.x

Wiederkehr M, Bousquet R, Schmid SM, Berger A (2008) From subduction to collision: thermal overprint of HP/LT meta-sediments in the north-eastern Lepontine Dome (Swiss Alps) and consequences regarding the tectono-metamorphic evolution of the Alpine orogenic wedge. Swiss J Geosci 101:127–155. https://doi.org/10.1007/s00015-008-1289-6

Wiederkehr M, Sudo M, Bousquet R et al (2009) Alpine orogenic evolution from subduction to collisional thermal overprint: the 40Ar/39Ar age constraints from the Valaisan Ocean, central

Alps. Tectonics 28:TC6009. https://doi.org/10.1029/2009TC002496

Zanchetta S (2010) The Texel-Schneeberg boundary in the Pfossen valley (Merano, NE Italy): geological-structural map and explanatory notes. Ital J Geosci 129:395–407. https://doi.org/10.3301/IJG.2010.13

Zangerl C, Loew S, Eberhardt E (2006) Structure, geometry and formation of brittle discontinuities in anisotropic crystalline rocks of the central Gotthard massif, Switzerland. Eclogae Geol Helv 99:271–290. https://doi.org/10.1007/s00015-006-1190-0

Zingg A, Handy MR, Hunziker JC, Schmid SM (1990) Tectonometamorphic history of the Ivrea zone and its relationship to the crustal evolution of the Southern Alps. Tectonophysics 182:169–192. https://doi.org/10.1016/0040-1951(90)90349-D

Zurbriggen R (2015) Ordovician orogeny in the Alps: a reappraisal. Int J Earth Sci 104:335–350. https://doi.org/10.1007/s00531-014-1090-x

Zurbriggen R (2017) The Cenerian orogeny (early Paleozoic) from the perspective of the Alpine region. Int J Earth Sci 106:517–529. https://doi.org/10.1007/s00531-016-1438-5

Zurbriggen R, Kamber BS, Handy MR, Nägler TF (1998) Dating synmagmatic folds: a case study of Schlingen structures in the Strona-Ceneri Zone (southern Alps, northern Italy). J Metamorph Geol 16:403–414. https://doi.org/10.1111/j.1525-1314.1998.00145